Journal of Advanced Research 61 (2024) 193–209

Contents lists available at ScienceDirect

Journal of Advanced Research

journal homepage: www.elsevier.com/locate/jare

ALKBH5 induces fibroblast-to-myofibroblast transformation during hypoxia to protect against cardiac rupture after myocardial infarction

Kun Yang [a,1], Yongchao Zhao [a,e,1], Jingjing Hu [a,f,1], Rifeng Gao [g,1], Jiaran Shi [f], Xiang Wei [g], Juntao Chen [h], Kai Hu [a], Aijun Sun [a,b,*], Junbo Ge [a,b,c,d,*]

[a] Department of Cardiology, Zhongshan Hospital, Fudan University, Shanghai Institute of Cardiovascular Diseases, China
[b] Institutes of Biomedical Sciences, Fudan University, Shanghai, China
[c] Key Laboratory of Viral Heart Diseases, National Health Commission, Shanghai, China
[d] Key Laboratory of Viral Heart Diseases, Chinese Academy of Medical Sciences, Shanghai, China
[e] Department of Cardiology, Affiliated Hospital of Zunyi Medical University, Guizhou Province, China
[f] Department of Cardiology, The First Affiliated Hospital, Zhejiang University School of Medicine, Zhejiang Province, China
[g] The Fifth People's Hospital of Shanghai, Fudan University, Shanghai, China
[h] Department of Urology, Zhongshan Hospital, Fudan University, Shanghai, China

HIGHLIGHTS

- ALKBH5 plays an important protective role during the post-MI repair phase.
- The loss of ALKBH5 in fibroblasts leads to cardiac rupture and deteriorated cardiac function.
- This study identities the ALKBH5 as hypoxia-related role in cardiac fibroblasts.
- ALKBH5 regulates fibroblast activation via *ErbB4* mRNA demethylation.
- ALKBH5/ErbB4 are possible therapeutic targets to reduce the occurrence of cardiac rupture.

GRAPHICAL ABSTRACT

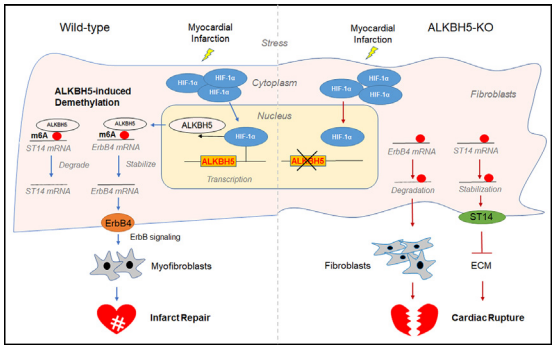

ARTICLE INFO

Article history:
Received 20 July 2023
Revised 4 September 2023
Accepted 6 September 2023
Available online 9 September 2023

Keywords:
m6A modification
ALKBH5
Myocardial infarction

ABSTRACT

Introduction: N6-methyladenosine (m6A) methylation produces a marked effect on cardiovascular diseases. The m6A demethylase AlkB homolog 5 (ALKBH5), as an m6A "eraser", is responsible for decreased m6A modification. However, its role in cardiac fibroblasts during the post-myocardial infarction (MI) healing process remains elusive.
Objectives: To investigate the effect of ALKBH5 in cardiac fibroblasts during infarct repair.
Methods: MI was mimicked by permanent left anterior descending artery ligation in global ALKBH5-knockout, ALKBH5-knockin, and fibroblast-specific ALKBH5-knockout mice to study the function of ALKBH5 during post-MI collagen repair. Methylated RNA immunoprecipitation sequencing was performed to explore potential ALKBH5 targets.

* Corresponding authors at: Department of Cardiology, Zhongshan Hospital, Fudan University, Shanghai Institute of Cardiovascular Diseases, 180 Fenglin Road, Shanghai 200032, China. Department of Cardiology, Zhongshan Hospital, Fudan University, Shanghai Institute of Cardiovascular Diseases, 180 Fenglin Road, Shanghai 200032, China.
E-mail addresses: sun.aijun@zs-hospital.sh.cn (A. Sun), jbge@zs-hospital.sh.cn (J. Ge).
[1] **These authors contributed equally to this work.**

https://doi.org/10.1016/j.jare.2023.09.004

Cardiac rupture
Hypoxia
ErbB4

Results: Dramatic alterations in ALKBH5 expression were observed during the early stages post-MI and in hypoxic fibroblasts. Global ALKBH5 knockin reduced infarct size and ameliorated cardiac function after MI. The global and fibroblast-specific ALKBH5-knockout mice both exhibited low survival rates along with poor collagen repair, impaired cardiac function, and cardiac rupture. Both *in vivo* and *in vitro* ALKBH5 loss resulted in impaired fibroblast activation and decreased collagen deposition. Additionally, hypoxia, but not TGF-β1 or Ang II, upregulated ALKBH5 expression in myofibroblasts by HIF-1α-dependent transcriptional regulation. Mechanistically, ALKBH5 promoted the stability of *ErbB4* mRNA and the degradation of *ST14* mRNA via m6A demethylation. Fibroblast-specific ErbB4 overexpression ameliorated the impaired fibroblast-to-myofibroblast transformation and poor post-MI repair due to ALKBH5 knockout.

Conclusion: Fibroblast ALKBH5 positively regulates post-MI healing by stabilization of *ErbB4* mRNA in an m6A-dependent manner. ALKBH5/ErbB4 might be potential therapeutic targets for post-MI cardiac rupture.

Introduction

Revascularization and widespread drug application during the early phase after acute myocardial infarction (MI) have greatly improved patient survival. However, after MI, patients have a substantial risk of a fatal complication known as cardiac rupture. Previous clinical research has reported that cardiac rupture often results in sudden death in the early stages of MI[1]. The transformation, proliferation, and migration of fibroblasts are key factors during post-MI healing for optimal scar formation to prevent cardiac rupture and adverse cardiac remodeling [1–3].

N6-methyladenosine (m6A) is the most abundant internal mRNA modification, which is dynamic and reversible [4]. It is catalytically installed by m6A methyltransferase complexes (the "writers"), such as methyltransferase-like 3 (METTL3) and methyltransferase-like 14 (METTL14), and their subunit proteins, Wilms tumor 1-associating protein (WTAP) and vir-like m6A methyltransferase-associated protein (VIRMA/ KIAA1429), and it is removed by m6A demethylases (the "erasers"), such as AlkB homolog 5 (ALKBH5) and the fat mass and obesity-associated gene (FTO). The m6A sites are recognized by specific RNA-binding proteins (the "readers"), such as YTH m6A RNA-binding proteins (YTHDFs) and insulin-like growth factor 2 mRNA-binding proteins (IGF2BPs). These proteins can affect mRNA splicing, localization, and stabilization as well as ribosomal accessibility, ultimately altering protein production [4–7]. In the cardiovascular field, previous findings have revealed decreased FTO expression along with subsequent cardiomyocyte contractile dysfunction in failing hearts. The role of the FTO-dependent m6A methylome has been defined in cardiomyocytes during heart failure [8], and cardiomyocyte-specific FTO loss injures cardiac function [9]. Accornero et al. [10] have identified METTL3-mediated mRNA m6A modification in response to cardiac hypertrophic stimulation. Song *et al.* [11] have uncovered an important link between METTL3/ALKBH5 and autophagy, offering valuable insights into m6A methylation and its regulators in cardiomyocytes after exposure to hypoxia and reoxygenation. Han et al. [12] have recently showcased the significant contribution of ALKBH5 in the control of cardiomyocyte proliferation and heart regeneration and that ALKBH5 overexpression improves cardiac function after MI. Our previous research has penetrated the effect of ALKBH5 in angiogenesis [13]. However, the role of ALKBH5 during post-MI healing remains unclear and warrants further investigation. Post-MI fibroblast-mediated collagen secretion and healing are crucial for preventing adverse cardiac remodeling and rupture. ALKBH5 might play an critical role in regulation of fibroblasts remodeling post-MI, therefore, we speculate that ALKBH5 might be a critical regulator of cardiac fibroblasts in the setting of ischemic myocardial insult.

In this study, m6A demethylase ALKBH5 is demonstrated as a crucial, hypoxia-related, cardioprotective factor that prevents post-MI cardiac remodeling and rupture by removing the m6A modification of *ErbB4* mRNA. In our experimental mouse model of MI, fibroblast-specific ALKBH5 knockout results in poor post-MI healing and increased mortality as well as cardiac dysfunction and rupture. Moreover, hypoxia, but not TGF-β1 or Ang II, induces ALKBH5 overexpression and promotes fibroblast-to-myofibroblast transformation via *ErbB4* mRNA stabilization in an m6A-dependent manner. Our novel discovery suggests targeting the ALKBH5/ErbB4 axis as a potential therapeutic strategy to facilitate infarct repair and prevent cardiac dysfunction and rupture.

Methods

Detailed experimental materials and methods are available in the Supplemental Methods.

Animals

Male C57BL/6 mice were purchased from Shanghai Laboratory Animal Research Center (Shanghai, China) and were housed at the Zhongshan Hospital, Fudan University. The mice were kept under a 12:12 h light/dark cycle, with consistent temperature and humidity, and ad libitum access to food and water. ALKBH5-knockout (KO) and -knockin (KI) mice were purchased from Gem Pharmatech (Nanjing, China). The heterozygous genotype line for deletion ALKBH5 was crossed to obtain KO mice and WT littermate control mice. WT control mice matched with KI were the same breeder pairs derived from KI heterozygous genotype line. The ALKBH5 immunofluorescence image and mRNA level in left ventricular myocardium of WT, KO and KI were shown in Supplement Fig. 9F. Col1α2^{creER} mice were crossed with ALKBH5$^{flox/flox}$ mice (Cyagen, China) to generate mice heterozygous for both alleles. Then ALKBH5$^{flox/flox}$ mice and heterozygous mice from the first cross produced ALKBH5$^{flox/flox}$Col1α2^{creER} mice, which were used in experiments. The 6-week-old ALKBH5$^{flox/flox}$Col1α2^{creER} mice were administration intraperitoneal injection of the tamoxifen suspension (30 mg/kg, Sigma-Aldrich) for 7 days. The ALKBH5$^{flox/flox}$ mice and Col1α2^{creER} mice as control were injected in in the same manner. The ALKBH5 immunofluorescence image in left ventricular myocardium of ALKBH5$^{flox/flox}$ and ALKBH5$^{flox/flox}$Col1α2^{creER} mice were shown in Supplement Fig. 9G**.**

Statistical analysis

Data were expressed as the mean ± standard deviation (SD) of at least three biological replicates. The normality of the data was esti-

mated using the Shapiro-Wilk test. $P < 0.05$ indicated significance. All statistical analysis was performed using SPSS 18.0 and GraphPad Prism 6.

Ethics statement

All experimental procedures complied with the ARRIVE guidelines, which were approved by the Animal Care Ethics Committee of the Zhongshan Hospital, Fudan University and were performed in accordance with the National Institutes of Health Guide for the Care and Use of Laboratory Animals.

Results

The m6A methylation involved in MI and the hypoxic response

The dot blot assay was performed to quantify the m6A levels of RNA extracted from the left ventricular remote non-ischemic, infarct border, and infarct areas at different timepoints after MI. The m6A levels remained unchanged at the remote non-ischemic area after MI (Fig. 1**A and 1D**). A sharp decrease in the m6A levels was observed as early as 3 days post-MI at the infarct border area and 1 day post-MI at the infarct area. The levels began to increase in the infarct area 7 days post-MI and in the infarct border area 14 days post-MI (Fig. 1**B-D**). To identify mediators of m6A modification during the post-MI phase, the expression levels of m6A methyltransferases, including METTL3 and METTL14, and m6A demethylases, including FTO and ALKBH5, were measured in the left ventricular remote non-ischemic, infarct border, and infarct areas (Fig. 1**E and 1H**). At the infarct border area, the protein levels of METTL14, METTL3 and FTO were slightly upregulated from day 1 to day 28 post MI. While the expression of ALKBH5 increased from day 1, peaked at day 5 post MI, and returned to baseline level at 28 days post MI. The unique ALKBH5 expression pattern in the border area may partially explain the similar trend observed in the m6A levels, in which the levels first decreased and then increased in these areas at different timepoints post-MI (Fig. 1**F and 1H**). In the infarct area, the expression of these four enzymes first decreased and then increased, and the turning point was on day 7 after MI (Fig. 1**G and 1H**).

We found that the m6A levels and the expression of m6A methylases markedly changed in response to MI, hinting the significant effect of m6A methylation on the post-MI process. Furthermore, the most drastic alteration occurred in demethylase ALKBH5 expression at the acute stage of MI.

ALKBH5 was upregulated in multiple cardiac cells in response to hypoxia

Cardiomyocytes and fibroblasts from neonatal mice were exposed to hypoxic conditions (1% O_2) at different timepoints, and we evaluated the m6A levels and the mRNA levels of methyltransferases and demethylases. The neonatal cardiomyocytes and fibroblasts were identified by immunofluorescence assay (Supplemental Fig. 1A). In cardiomyocytes, hypoxia initially increased and then decreased the mRNA expression of m6A methylases, among which *Wtap, Kiaa1429*, and *Alkbh5* exhibited the most remarkable changes in expression (Supplemental Fig. 1B). In cardiac fibroblasts, hypoxia stimulated the most significant increase in *Alkbh5* expression, whereas the expression of the other enzymes showed either a slight upregulation or no difference at all (Supplemental Fig. 1C). Additionally, we found that the m6A levels gradually decreased with increased exposure time to hypoxia in fibroblasts (Supplemental Fig. 1D). And the hypoxia 24 h increased ALKBH5 mRNA expression in CMECs and macrophages compared with normoxia (Supplemental Fig. 1E). Collectively, these data suggested that the differential expression of ALKBH5 may be a vital molecular hallmark in hypoxic cardiac cells after MI. Therefore, we continued to explore the effect of ALKBH5 in response to MI.

Global ALKBH5 overexpression ameliorated cardiac function after MI

The ALKBH5- knockin (KI) mice were generated using the CRISPR/Cas9 technology (Supplemental Fig. 2A), as detailed in Supplement 1. Western blot analysis demonstrated that ALKBH5 expression in the heart, liver, and kidneys was markedly increased in the ALKBH5-KI mice contrast in the wild-type (WT) mice (Supplemental Fig. 2B). Dot blot assay showed lower m6A levels in RNA extracted from the hearts of the ALKBH5-KI mice contrast in that from the hearts of the WT mice (Supplemental Fig. 3A). No significant differences were observed between the echocardiographic parameters of the ALKBH5-KI and WT mice (Supplemental Fig. 3C). Hematoxylin and eosin (H&E) and Masson's trichrome staining of heart tissue sections showed no morphological differences between the ALKBH5-KI and WT mice, and similar results were obtained from the liver and kidney tissue sections (Supplemental Fig. 3D).

Next, we performed left coronary artery ligation or sham surgery in the ALKBH5-KI and WT mice. A 100% survival rate was observed in both the sham-operated WT (n = 7) and ALKBH5-KI (n = 7) mice. Furthermore, no difference was observed between the survival rates (85%, n = 20 vs. 87.5%, n = 16) of the WT and ALKBH5-KI mice 28 days after MI surgery (Supplemental Fig. 2C). The occurrence of death caused by cardiac rupture was 6.25% (1/16) in the ALKBH5-KI mice after MI surgery, whereas it was 10% (2/20) in the WT mice (Supplemental Fig. 2D). Echocardiography analysis was performed at day 1 post-MI, ALKBH5-KI and WT mice with similar ejection fraction were chosen for further studies (Supplemental Fig. 3E). Masson's trichrome staining revealed that the ALKBH5-KI mice exhibited smaller infarct areas, less collagen deposition, and increased cardiac wall thinning after MI surgery, indicating enhanced post-MI repair and reduced fibrosis (Supplemental Fig. 2E and 2F)**.** As expected, echocardiographic analysis demonstrated that the ALKBH5-KI mice exhibited less left ventricular dilation and ameliorative cardiac function contrast in the WT mice after MI surgery (Supplemental Fig. 2G and 2H; Supplemental Table 1).

ALKBH5 deficiency exacerbated post-MI mortality and cardiac rupture, remodeling, and dysfunction

The ALKBH5-knockout (KO) mice were constructed using the CRISPR/Cas9 technology (Fig. 2**A**), as described in Supplement 2. Compared with the WT mice, the ALKBH5-KO mice displayed successful deletion of the *Alkbh5* gene in the heart, liver, and kidneys (Fig. 2**B**). Dot blot assay revealed that RNA extracted from the hearts of the ALKBH5-KO mice had higher m6A levels compared with that from the hearts of the WT mice (Supplemental Fig. 3B). Echocardiography showed no differences between the WT and ALKBH5-KO mice under physiological conditions (Supplemental Fig. 3C). H&E and Masson's trichrome staining of heart tissue sections showed no significant differences in myocardial size and arrangement or collagen deposition between the WT and ALKBH5-KO mice. There were also no morphological differences in the liver and kidney tissues (Supplemental Fig. 3D).

To study the function of ALKBH5 in MI, we performed left coronary artery ligation or sham surgery in WT and ALKBH5-KO mice. A 100% survival rate was observed in both the sham-operated WT (n = 7) and ALKBH5-KO (n = 7) mice after 28 days. However, compared with the WT mice (86.1%, survival n = 31, total n = 36), the survival rate of the ALKBH5-KO mice (65.4%, survival n = 17, total

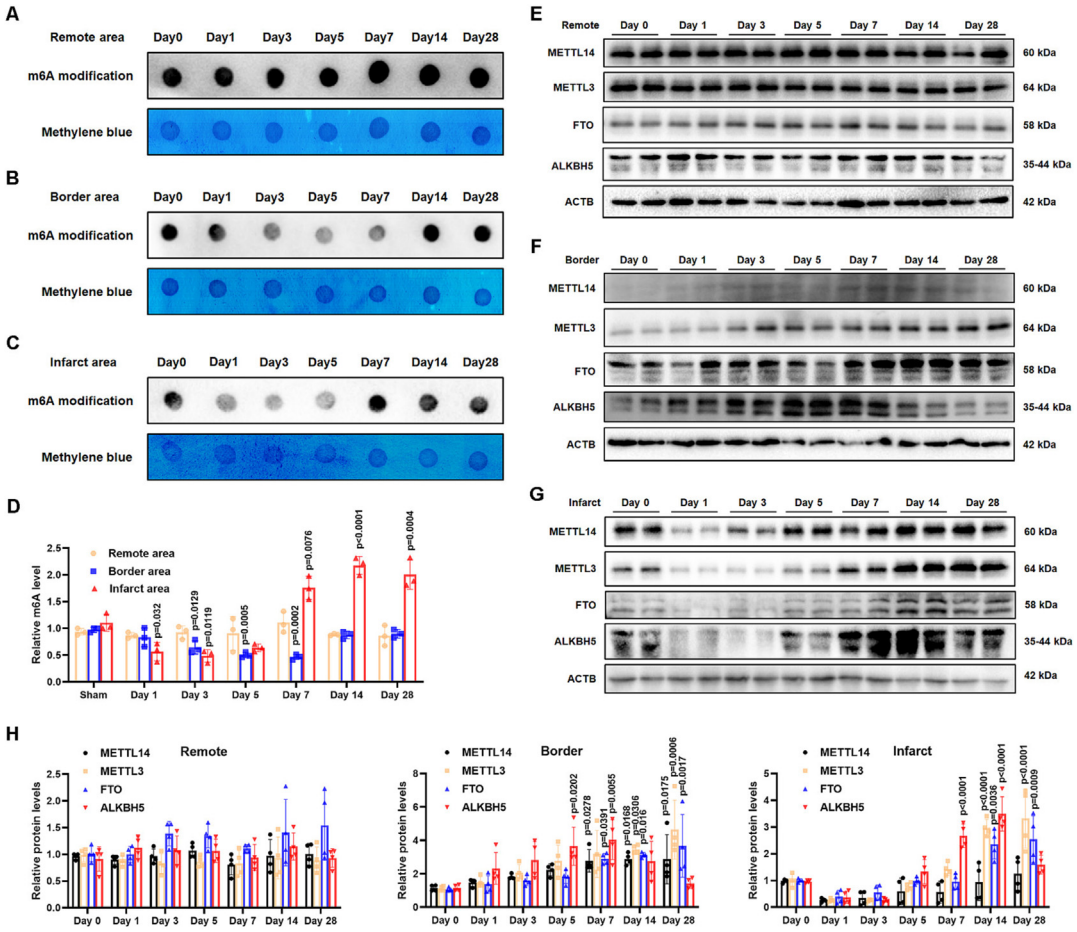

Fig. 1. The levels of m6A modification and m6A-related modification enzyme expression changes after MI Left coronary artery ligation surgery was performed in wild-type mice. In the sham-operated group, the hearts were exposed but not subjected to LCAL (n = 4 in the sham-operated group and n = 28 in the LCAL-operated group). All hearts in the LCAL-operated and the sham-operated group were collected at different time after surgery. The levels of m6A modification from the remote non-ischemic area **(A)**, infarct border area **(B)** and the infarct area **(C)**. **(D)** Quantification of m6A modification (n = 3 per group, One-Way ANOVA using Tukey test). The protein expression of METTL3, METTL14, FTO and ALKBH5 from the remote non-ischemic area **(E)**, infarct border area **(F)** and the infarct area **(G)** was detected by Western blot assay. **(H)** Quantification of METTL3, METTL14, FTO and ALKBH5 protein levels (n = 4 per group, One-Way ANOVA using Tukey test). The data were presented as the means ± SD of four independent experiments.

n = 26) was significantly lower 28 days after MI surgery ($P < 0.001$) (Fig. 2**C**). Additionally, these deaths occurred earlier in the ALKBH5-KO mice than in the WT mice. Autopsies revealed that almost all of the deceased mice in both groups showed signs of cardiac rupture, including blood coagulation in the chest cavities and small tears in the left ventricular walls (Fig. 2**D**). The incidence of post-MI cardiac rupture in ALKBH5-KO mice was significantly higher than that in WT mice (34.6%, 9/26 vs. 11.1%, 4/36) (Fig. 2**E**). Echocardiographic analysis 1 day after MI surgery showed no significant differences between the ALKBH5-KO and WT mice (Supplemental Fig. 3F). H&E and Masson's trichrome staining revealed that ALKBH5 deficiency resulted in exacerbated cardiac wall thinning and lower collagen deposition at the infarct area 28 days after MI surgery, whereas there was no difference in infarct size (%) between the ALKBH5-KO and WT mice (Fig. 2**F and 2G**). Western blot analysis showed that the protein levels of Col1α1 and α-SMA were significantly reduced in the infarct areas of the ALKBH5-KO mice 28 days post-MI in contrast to those of WT mice (Fig. 2**H**). The m6A levels in the infarct area tissues from the ALKBH5-KO group 28 days post-MI were higher than those of the WT mice (Fig. 2**I**). Cardiac function was analyzed 7, 14, and 28 days after MI surgery. Intriguingly, the echocardiographic analysis demonstrated exacerbated adverse cardiac remodeling, including left ventricular wall thinning, increased left ventricular internal diameter, and left ventricular systolic dysfunction, in the ALKBH5-KO mice in contrast to that of the WT mice (Fig. 2**J and 2K;** Supplemental Table 2).

Global ALKBH5 knockout reduced scar formation after MI

The excessive early inflammatory and weakened scar repair processes are the causes of cardiac rupture. The myofibroblast activation was analyzed between the ALKBH5-KO and WT mice 5 days a post-MI because of the peak time of cardiac rupture. The m6A levels in the infarct area tissues from the ALKBH5-KO mice were higher than those of the WT mice (Fig. 3**A**). The protein levels of Col1α1 and α-SMA were significantly decreased in the infarct areas of the ALKBH5-KO mice compared with the WT mice, whereas the levels of MMP2 and MMP9 were increased (Fig. 3**B**). Furthermore, increased mRNA levels of *Mmp2*, *Mmp3*, and *Mmp9* and decreased levels of *α-SMA*, *Col1α1*, and *Col3α1* were detected in the infarct areas of the ALKBH5-KO mice compared with those of the WT mice (Fig. 3**C**). Immunofluorescence staining for Collagen I and Collagen III revealed significantly reduced collagen in the infarct border and infarct areas of the ALKBH5-KO mice compared with those of the WT mice (Fig. 3**D**). Additionally, less α-SMA and proliferating myofibroblasts (α-SMA$^+$Ki67$^+$ double-positive cells) were assessed

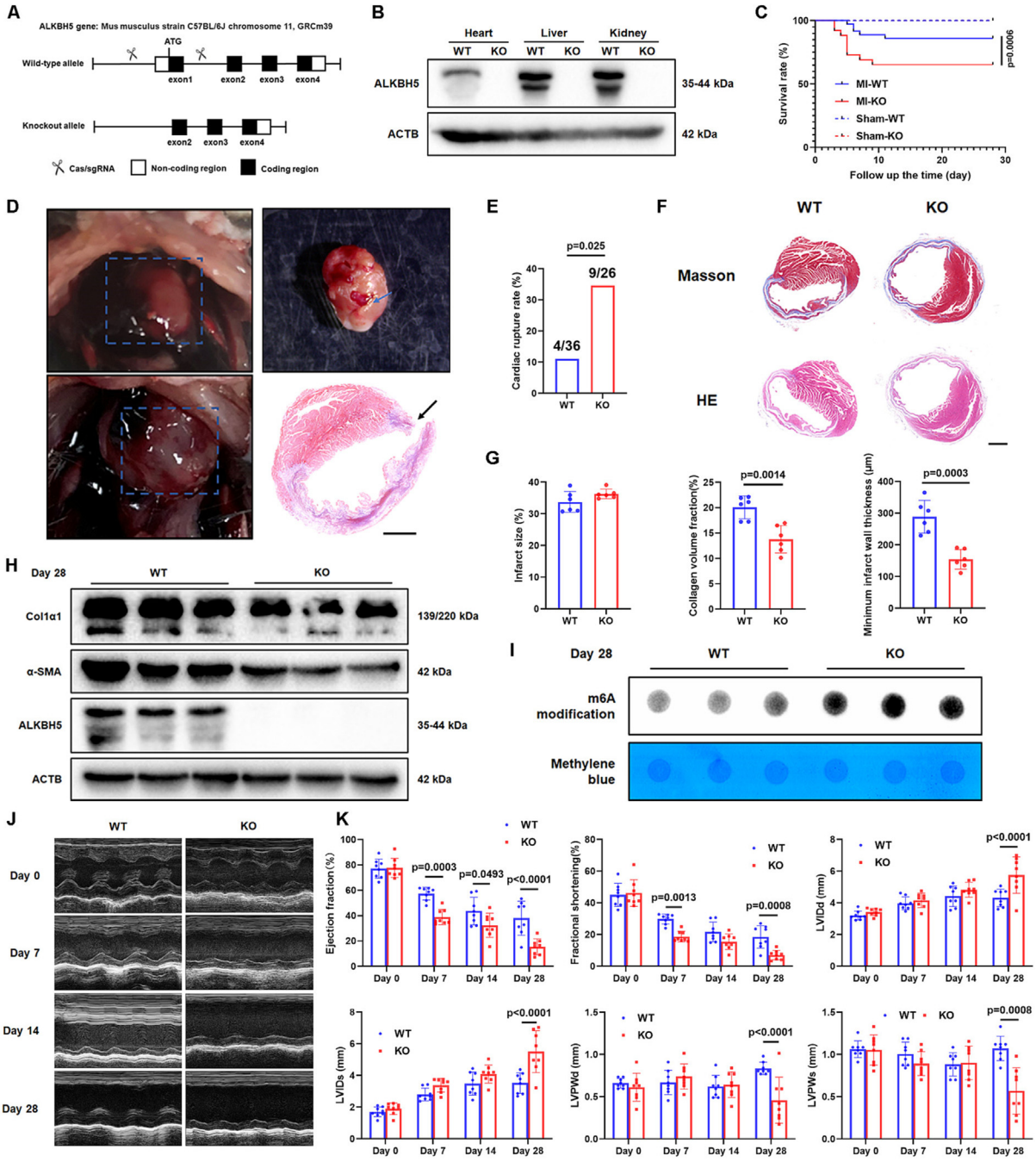

Fig. 2. ALKBH5 deficiency exacerbated cardiac rupture, remodeling, and dysfunction caused by MI Left coronary artery ligation surgery was performed in WT and KO mice. In the sham-operated group, the hearts were exposed but not subjected to LCAL (n = 7 in sham-operated WT and KO group. n = 36 in LCAL-operated WT group and n = 26 in LCAL-operated KO group). **(A)** The construction strategy of ALKBH5-knockout mice was shown. **(B)** Western blot assay was performed to demonstrate the successful deletion of the ALKBH5 gene in the heart, liver and kidney. **(C)** The survival curve of MI-WT and MI-KO groups from the day of left coronary artery ligation until postoperative 28 days (MI-WT group n = 36 vs MI-KO group n = 26, Log-rank test). **(D)** Representative images of autopsy and HE staining of cardiac rupture section. Scale bars, 1 mm. **(E)** The occurrence of death caused by cardiac rupture in MI-WT and MI-KO groups (chi-square test). **(F)** Representative images of Masson's trichrome staining and HE staining of ventricular sections of MI-WT and MI-KO 28 days after myocardial infarction and **(G)** the analysis of infarct size, collagen volume fraction and minimum infarct wall thickness (n = 6 per group, Unpaired two-tailed Student's *t*-test).Scale bars, 1 mm. **(H)** The protein levels of ALKBH5, Col1α1 and α-SMA were measured in the infarct area of hearts of WT and KO groups 28 days after MI by Western blot analysis. **(I)** The levels of m6A modification were assessed in the infarct area of hearts of WT and KO groups 28 days after MI by Dot blot assay. **(J and K)** Echocardiography was performed to assess EF and FS of the left ventricle in MI-WT and MI-KO groups at sham, days 7, 14 and 28 post-MI (n = 8 per group, Two-Way ANOVA using Šídák's multiple comparisons test).

per field in the infarct border and infarct areas of the ALKBH5-KO mice in contrast to those of the WT mice (Fig. 3**E**).

Next, inflammatory cell infiltration ($CD68^+$ macrophages and $Ly6G^+$ neutrophils) was evaluated after MI. The number of $Ly6G^+$ neutrophils increased in the hearts of the ALKBH5-KO and WT mice 1, 3, and 5 days post-MI. The highest number of these cells was detected on day 3, particularly in the infarct border areas, compared with the corresponding sham-operated hearts. Moreover, the number of $Ly6G^+$ neutrophils in the infarct border and infarct areas of the ALKBH5-KO mice was slightly less than that of the WT mice, but this statistical difference only existed in the infarct border area on day 3 (Fig. 3**F**). In contrast, $CD68^+$ macrophage infil-

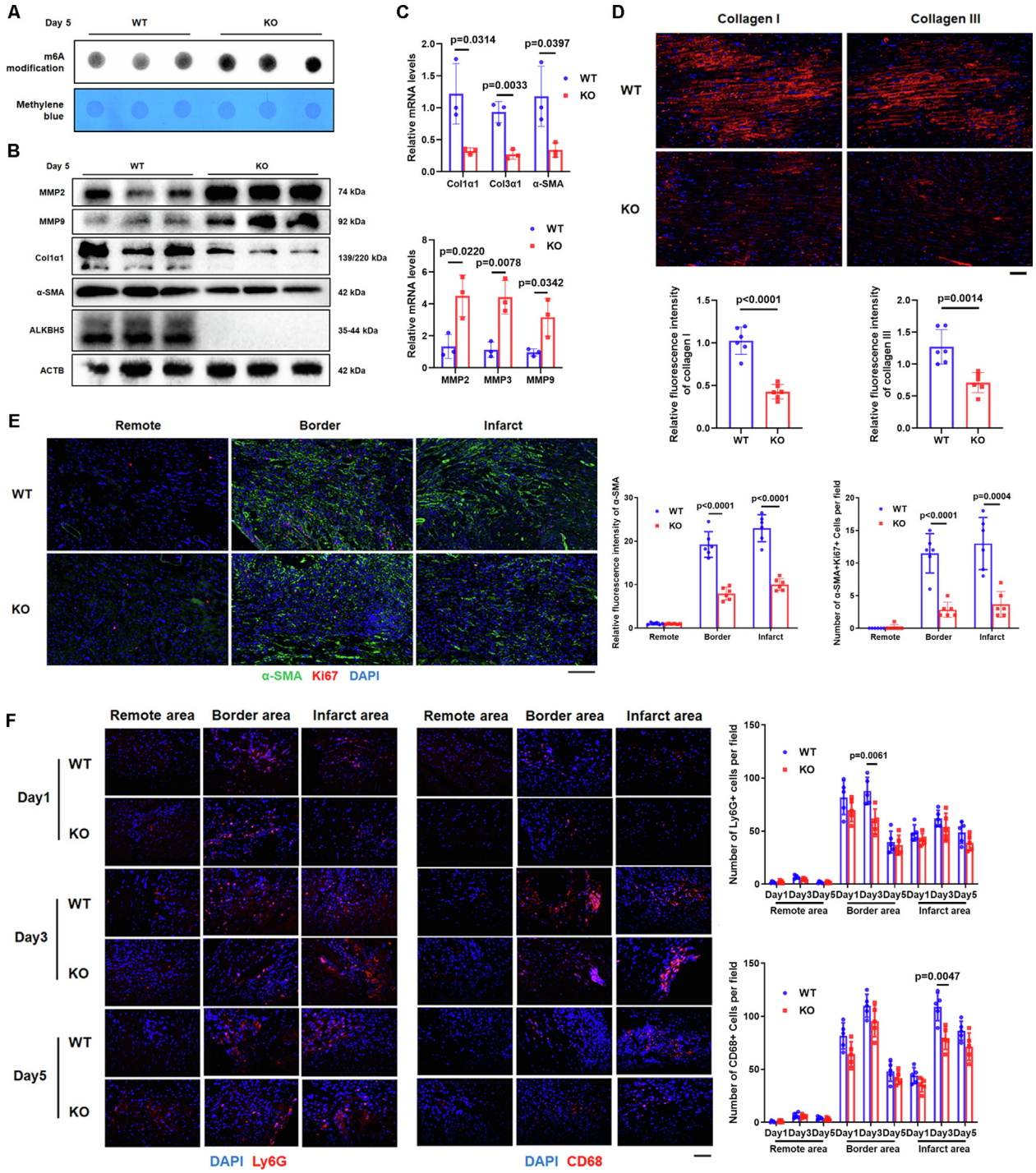

Fig. 3. The global deletion of ALKBH5 reduced scar formation after MI (A) The levels of m6A modification were assessed in the infarct area of hearts of WT and KO groups 5 days after MI by Dot blot assay. **(B)** The protein of ALKBH5, Col1α1, α-SMA, MMP2 and MMP9 were measured in the infarct area of hearts of WT and KO groups 5 days after MI by Western blot analysis. **(C)** The mRNA levels of ALKBH5, Col1α1, Col3α1, α-SMA, MMP2, MMP3 and MMP9 were measured in the infarct area of hearts of WT and KO groups 5 days after MI by RT-qPCR (n = 3 per group, Unpaired two-tailed Student's *t*-test). **(D)** Immunofluorescence staining and quantification of Collagen I and Collagen III in border areas of the WT and ALKBH5-KO mice 5 days after MI (n = 6 per group, Unpaired two-tailed Student's *t*-test). Scale bars, 50 μm. **(E)** Immunofluorescence staining of α-SMA and Ki67 in remote, border, and infarction areas of the WT and ALKBH5-KO mice 5 days after MI. Quantification of α-SMA fluorescence intensity and the number of α-SMA$^+$Ki67$^+$ cells per field (n = 6 per group, Unpaired two-tailed Student's *t*-test).Scale bars, 50 μm **(F)** Representative images of immunofluorescence staining of CD68$^+$ macrophages and Ly6G$^+$ neutrophils in left ventricle of Sham-WT and Sham-KO groups. Immunofluorescence staining of CD68$^+$ macrophages and Ly6G$^+$ neutrophils in the remote, border, and infarction areas of the WT and ALKBH5-KO mice 1, 3, and 5 days after MI (n = 5 per group, Unpaired two-tailed Student's *t*-test). Scale bars, 50 μm.

tration increased in the infarct border and infarct areas of both the ALKBH5-KO and WT hearts 1 and 3 days after MI surgery, but there was a decrease in this observation by day 5. The number of infiltrated CD68$^+$ macrophages in the infarct border and infarct areas of the ALKBH5-KO mice was slightly less than that of the WT mice, but this statistical difference only existed in the infarct area on day 3 (Fig. 3**F**). In addition, we evaluated the role of ALKBH5 in angiogenesis after MI. *In vitro*, ALKBH5 knockout using si-ALKBH5 pro-

moted endothelial cell proliferation, migration, and tube formation (Supplemental Fig. 4A-F). *In vivo*, CD31 immunofluorescence staining was used to evaluate angiogenesis in the MI mouse models. The global ALKBH5-KO mice exhibited improved angiogenesis, whereas the global ALKBH5-KI mice exhibited impaired angiogenesis (Supplemental Fig. 4G and 4H).

These results indicated that ALKBH5 deficiency impaired the scar repair process mainly by inhibition of cardiac fibroblast activation after MI.

Loss of ALKBH5 in fibroblasts led to cardiac rupture after MI

To demonstrate that the loss of ALKBH5 in fibroblasts leads to cardiac rupture, we crossed ALKBH5$^{flox/flox}$ mice with Col1α2^{creER} mice. Detailed information on the generation and genotyping of these mice has been provided in Supplement 3. The ALKBH5$^{flox/flox}$-Col1α2^{creER} mice were injected with tamoxifen (30 mg/kg) for 7 days prior to MI surgery to induce the cardiac fibroblast-specific disruption of ALKBH5 expression (Fig. 4**A**). Then, the *Alkbh5* mRNA levels were detected in cardiomyocytes and cardiac fibroblasts isolated from the hearts of ALKBH5$^{flox/flox}$ and ALKBH5$^{flox/flox}$Col1α2^{creER} mice after tamoxifen treatment. RT-qPCR analysis indicated that the *Alkbh5* mRNA levels were significantly decreased in fibroblasts, but not in cardiomyocytes, from the ALKBH5$^{flox/flox}$Col1α2^{creER} mice (Fig. 4**B**). There were no differences in cardiac function between the ALKBH5$^{flox/flox}$ and ALKBH5$^{flox/flox}$Col1α2^{creER} mice under physiological conditions by echocardiography 7 days after tamoxifen treatment (Supplemental Fig. 5A). And H&E and Masson's trichrome staining of heart tissue sections also showed no significant differences in myocardial size and arrangement or collagen deposition between the ALKBH5$^{flox/flox}$ and ALKBH5$^{flox/flox}$-Col1α2^{creER} mice (Supplemental Fig. 5B).

We performed left coronary artery ligation or sham surgery in ALKBH5$^{flox/flox}$, Col1α2^{creER}, and ALKBH5$^{flox/flox}$Col1α2^{creER} mice. Compared with the ALKBH5$^{flox/flox}$ mice (92.9%, n = 28) and Col1α2^{creER} mice (89.7%, n = 29), the ALKBH5$^{flox/flox}$Col1α2^{creER} mice (66.6%, n = 33) exhibited a significantly lower survival rate 28 days after MI surgery ($P < 0.001$) (Fig. 4**C**). Autopsies showed that almost all of the deceased mice in both groups showed signs of cardiac rupture, including blood coagulation in the chest cavities and small tears in the left ventricular walls (Fig. 4**D**). The incidence of post-MI cardiac rupture was significantly higher in the ALKBH5$^{flox/flox}$Col1α2^{creER} mice than in the ALKBH5$^{flox/flox}$ and Col1α2^{creER} mice (30.3%, 10/33 vs. 7.1%, 2/28 vs. 10.3%, 3/29) (Fig. 4**E**). There were no differences in cardiac function 1 day post-MI (Supplemental Fig. 5C) between the ALKBH5$^{flox/flox}$ and ALKBH5$^{flox/flox}$Col1α2^{creER} mice. Because there were no differences in post-MI mortality or cardiac rupture rate between the ALKBH5$^{flox/flox}$ and Col1α2^{creER} mice, the ALKBH5$^{flox/flox}$ mice were used as the control group. Next, the protein levels of MMP2, MMP9, Col1α1, and α-SMA and the mRNA levels of *Mmp2, Mmp3, Mmp9, α-Sma, Col1α1*, and *Col3α1* were evaluated. Compared with the ALKBH5$^{flox/flox}$ controls, the ALKBH5$^{flox/flox}$-Col1α2^{creER} mice exhibited elevated MMP expression and reduced collagen repair marker expression after MI surgery (Fig. 4**F**; Supplemental Fig. 5D). Immunofluorescence staining of the infarct areas 5 days post-MI showed that the ALKBH5$^{flox/flox}$Col1α2^{creER} mice exhibited lower Collagen I, Collagen III, and α-SMA levels as well as a lower number of proliferating myofibroblasts per field than the ALKBH5$^{flox/flox}$ mice (Fig. 4**G and 4H**). Histological analysis of cardiac tissues from the fibroblast-specific ALKBH5-KO mice revealed less collagen deposition and an overall smaller minimum wall thickness in the injury region 28 days post-MI in contrast to those of the controls. However, there was no difference in infarct size (%) between the two groups (Fig. 4**I**; Supplemental Fig. 5E and 5F). Echocardiographic analysis demonstrated impaired cardiac function and left ventricular dilation in the ALKBH5$^{flox/flox}$-Col1α2^{creER} mice compared with the ALKBH5$^{flox/flox}$ mice 7, 14, and 28 days post-MI (Fig. 4**J**; Supplemental Fig. 5G; Supplemental Table 3). These findings strongly indicated the regulation of ALKBH5 in cardiac fibroblast-mediated scar repair after MI.

Hypoxia, but not TGF-β1 or Ang II, upregulated ALKBH5 expression in myofibroblasts in a HIF-1α-dependent transcriptional manner

Hypoxia, TGF-β1, and Ang II are essential inducers of the fibroblast-to-myofibroblast transformation. Therefore, fibroblasts were either exposed to hypoxia or treated with TGF-β1 or Ang II for 48 h. As expected, the mRNA levels of major myofibroblast markers, *Col1α1, α-Sma*, fibronectin (*Fn*), and connective tissue growth factor (*Ctgf*), were drastically upregulated (Supplemental Fig. 6A). However, only hypoxic stimulation caused an increase in the expression levels of *Alkbh5* mRNA (Fig. 5**A and 5B**).

Next, we generated a luciferase reporter pGL3 plasmid controlled by the murine *Alkbh5* promoter (-2,000-+200 bp; pGL3-Promoter). NIH/3T3 cells were co-transfected with either pGL3-Promoter or control (pGL3-Empty) plasmid along with Renilla luciferase plasmid. Hypoxia activated the luciferase activity of the pGL3-Promoter plasmid (Fig. 5**C**), whereas treatment with TGF-β1 or Ang II had no effect (Fig. 5**D**). Western blot analysis confirmed that the protein expression levels of ALKBH5 gradually increased under hypoxic conditions from 0 to 48 h, along with HIF-1α, Col1α1, and α-SMA (Fig. 5**E**).

Previous researches have reported that hypoxia elevated ALKBH5 expression in breast cancer cells and Escherichia coli via HIF-1α-induced transcriptional regulation [14,15]. Therefore, we postulated that ALKBH5 may be transcriptionally activated by HIF-1α under hypoxic conditions in fibroblasts. The fibroblasts were transfected with siRNA against HIF-1α or control siRNA. The silencing of HIF-1α blocked the hypoxia-induced increase in HIF-1α, ALKBH5, α-SMA, and Col1α1 expression (Supplemental Fig. 6C). The JASPAR (jaspar.genereg.net) website indicated that 22 hypoxia response elements (HREs) were predicted to bind to the promoter region of the murine *Alkbh5* gene (Supplemental Fig. 6C). The Cistrome Data Browser (cistrome.org) revealed peak signals within the HIF-1α binding site of the *Alkbh5* promoter region using previously generated ChIP-seq datasets [16] (Supplemental Fig. 6C). HIF-1α was shown to prefer the conserved binding site (5′-RCGTG-3′, R = A or G) on the *Alkbh5* promoter (Fig. 5F), which was consistent with the HIF-1α peak signal provided by the ChIP-seq database (Supplemental Fig. 6C). To determine whether HIF-1α directly binds to *Alkbh5* during transcription, ChIP assay was performed using either a HIF-1α or IgG control antibody in fibroblasts after exposure to normoxic or hypoxic conditions (Fig. 5G). The *Alkbh5* promoter fragment A, but not fragment B, was preferentially enriched after immunoprecipitation with the HIF-1α antibody compared with the IgG control antibody under both normoxic and hypoxic conditions. Moreover, an increased amount of the *Alkbh5* promoter fragment A was immunoprecipitated with the HIF-1α antibody after exposure to hypoxia (Fig. 5H). NIH/3T3 cells were co-transfected with either pGL3-Promoter or pGL3-Empty plasmid and the Renilla luciferase plasmid. Exposure to hypoxia activated the luciferase activity of the pGL3-Promoter plasmid, whereas transfection with si-HIF-1α (si-HIF-1α-1, si-HIF-1–2) significantly inhibited this effect (Fig. 5I).

Collectively, our data showed that hypoxia, but not TGF-β1 or Ang II, upregulated ALKBH5 expression in cardiac fibroblasts. This effect required the constitutive binding of HIF-1α to the HREs within the *Alkbh5* promoter, suggesting hypoxia as a transcriptional regulator of *Alkbh5*.

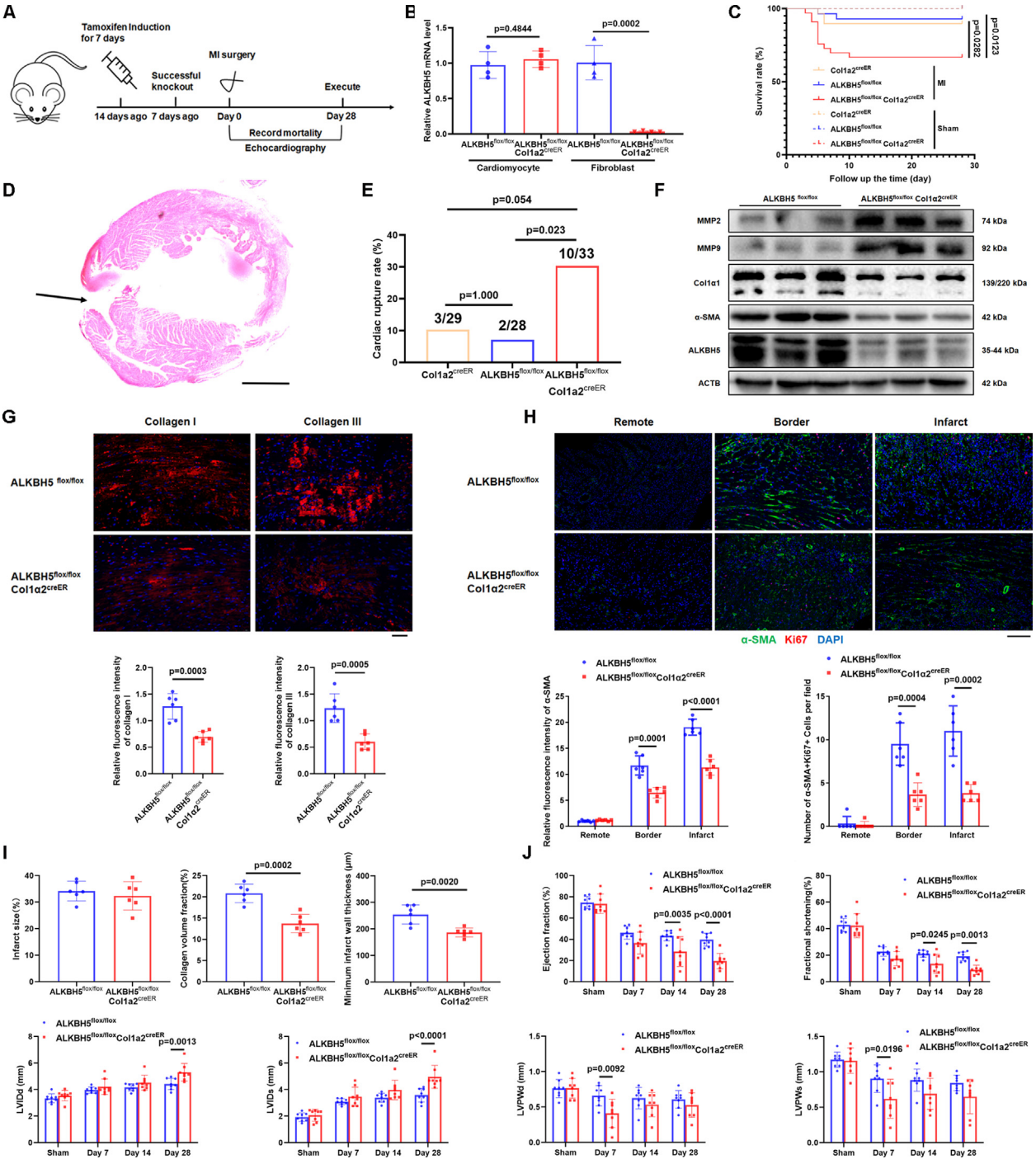

Fig. 4. Loss of ALKBH5 in fibroblasts leads to cardiac rupture after MI MI surgery was performed in ALKBH5$^{flox/flox}$ mice and ALKBH5$^{flox/flox}$Col1α2^{creER} mice. (n = 28 in LCAL-operated ALKBH5$^{flox/flox}$ group, n = 29 in LCAL-operated Col1α2^{creER} mice and n = 33 in LCAL-operated ALKBH5$^{flox/flox}$Col1α2^{creER} group). **(A)** Experimental strategy of myocardial infarction model in ALKBH5$^{flox/flox}$ mice and ALKBH5$^{flox/flox}$Col1α2^{creER} mice. **(B)** The mRNA level of ALKBH5 in cardiomyocytes and fibroblasts isolated from ALKBH5$^{flox/flox}$ mice and ALKBH5$^{flox/flox}$Col1α2^{creER} mice by RT-qPCR (n = 4 per group, Unpaired two-tailed Student's *t*-test). **(C)** The survival curve of ALKBH5$^{flox/flox}$ group, Col1α2^{creER} group and ALKBH5$^{flox/flox}$Col1α2^{creER} group from the day of left coronary artery ligation until postoperative 28 days (ALKBH5$^{flox/flox}$ group n = 28 vs Col1α2^{creER} mice n = 29 vs ALKBH5$^{flox/flox}$Col1α2^{creER} group n = 33, Log-rank test). **(D)** Representative images HE staining of cardiac rupture section. **(E)**The occurrence of death caused by cardiac rupture in ALKBH5$^{flox/flox}$ group, Col1α2^{creER} group and ALKBH5$^{flox/flox}$Col1α2^{creER} group (fisher's exact test or chi-square test).Scale bars, 1 mm. **(F)** The protein levels of ALKBH5, Col1α1, α-SMA, MMP2 and MMP9 were measured in the infarct area of hearts of ALKBH5$^{flox/flox}$ group and ALKBH5$^{flox/flox}$Col1α2^{creER} group 5 days after MI by Western blot analysis. **(G)** Representative diagram and quantification of fluorescence intensity of collagen I and collagen III (n = 6 per group, Unpaired two-tailed Student's *t*-test). Scale bars, 50 μm **(H)** Representative diagram and quantification of fluorescence intensity of α-SMA fluorescence intensity and the number of α-SMA^{+} Ki67^{+} cells per field (n = 6 per group, Unpaired two-tailed Student's *t*-test). Scale bars, 50 μm. **(I)**The analysis of collagen volume fraction and minimum wall thickness from Masson's trichrome staining of ventricular sections of ALKBH5$^{flox/flox}$ group and ALKBH5$^{flox/flox}$Col1α2^{creER} group 28 days after myocardial infarction (n = 6 per group, Unpaired two-tailed Student's *t*-test). **(J)** Echocardiography was performed to assess EF and FS of the left ventricle in ALKBH5$^{flox/flox}$ group and ALKBH5$^{flox/flox}$Col1α2^{creER} group at days sham 7, 14 and 28 post-MI (n = 8 per group, Two-Way ANOVA using Šídák's multiple comparisons test).

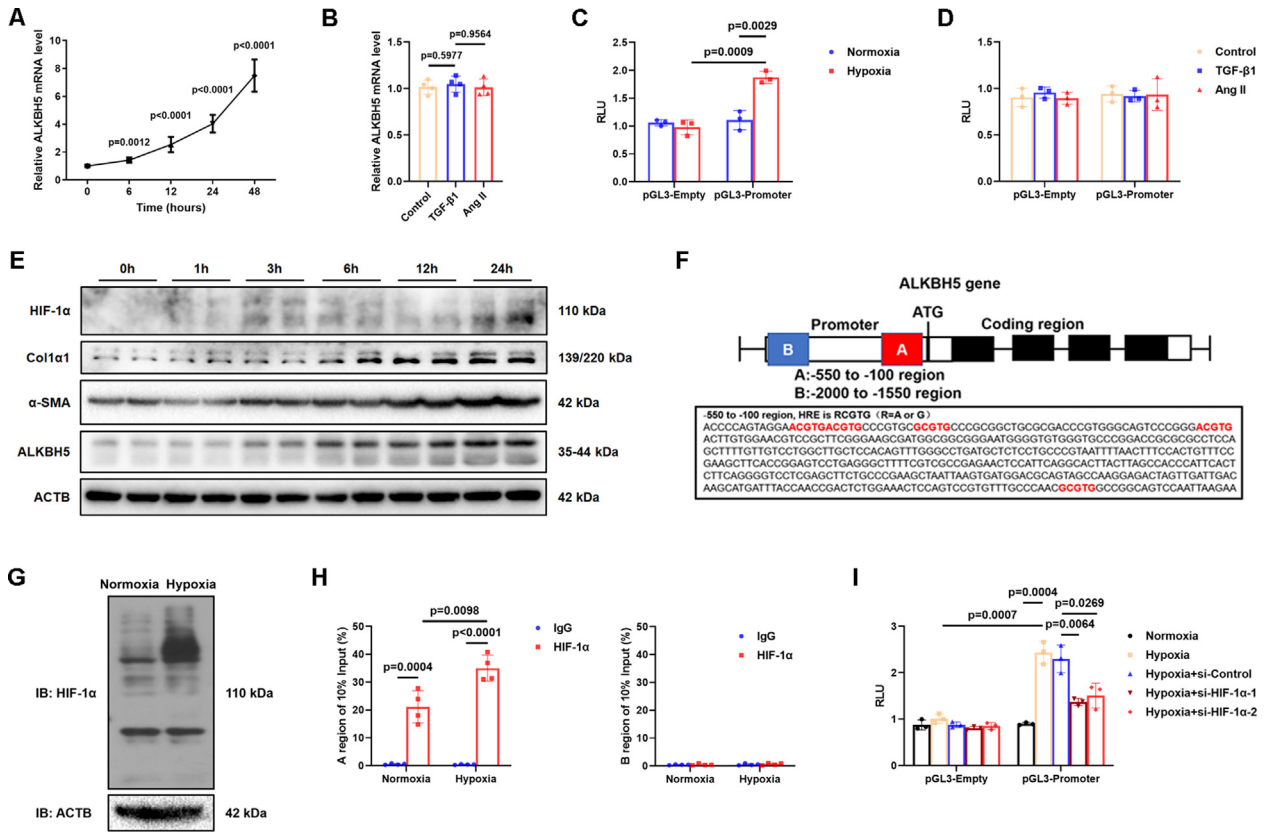

Fig. 5. Hypoxia transcriptionally up-regulates ALKBH5 expression by HIF-1α 10 ng/ml TGF-β1 or 100 nM Ang-II was treated with fibroblasts for 48 h compared with vehicle (1% BSA). **(A and B)** Fibroblasts were exposed to hypoxia (1% oxygen) or normoxia for a different time (n = 3 per group, Unpaired two-tailed Student's *t*-test). RT-qPCR was performed to detect the mRNA level of ALKBH5 (n = 4 per group, Unpaired two-tailed Student's *t*-test). **(C and D)** Dual-luciferase reporter assay was performed after co-transfection with a reporter vector in NIH/3T3 (n = 3 per group, Unpaired two-tailed Student's *t*-test). **(E)** The protein levels of ALKBH5, HIF-1α, VEGFA, Col1α1 and α-SMA in hypoxic and normoxic fibroblasts were measured by Western blot assay. **(F)** HIF-1α preferred binding site (5′-RCGTG-3′, R = A or G) on ALKBH5 promoter was shown. A region is a potential binding sequence while a B region is as control. ChIP analysis of fibroblasts pretreated with hypoxia (1% oxygen) or normoxia for 48 h. **(G)** Western blot analysis of input proteins and proteins immunoprecipitated with either HIF-1α antibody or IgG. The input proteins were standardized by the ACTB level. **(H)** Immunoprecipitation products were measured by RT-qPCR (n = 4 per group, Unpaired two-tailed Student's *t*-test). **(I)** Dual-luciferase reporter assay was performed after co-transfection with a reporter vector and Si-HIF-1α or Si-Control in NIH/3T3 under hypoxia or normoxia for 48 h (n = 3 per group, Unpaired two-tailed Student's *t*-test).

ALKBH5 promoted fibroblast proliferation, migration, and transformation into myofibroblasts

Adenoviral vectors were used to overexpress (Ad-ALKBH5) or knockdown (Ad-sh-ALKBH5-1, Ad-sh-ALKBH5-2, Ad-sh-ALKBH5-3) ALKBH5 expression in neonatal mouse fibroblasts (Supplemental Fig. 6D). We used Ad-sh-ALKBH5-3 for subsequent experiments because it exhibited the highest knockdown efficiency. The m6A levels were significantly decreased in fibroblasts transduced with Ad-ALKBH5. However, the m6A levels were significantly elevated after transduction with Ad-sh-ALKBH5 (Supplemental Fig. 6E).

CCK-8 and EdU assays were performed to estimate the role of ALKBH5 on the proliferative capacity of fibroblasts, and the migratory capacity of fibroblasts was detected by a transwell assay. Compared with transduction with Ad-Control, ALKBH5 overexpression markedly promoted fibroblast proliferation and migration, whereas ALKBH5 knockdown inhibited this effect (Supplemental Fig. 6F; Fig. 6A–D). Similarly, we evaluated the role of ALKBH5 in fibroblast proliferation and migration under hypoxia. Overexpression of ALKBH5 enhanced the proliferative and migratory capacities of fibroblasts in response to hypoxia, whereas ALKBH5 knockdown impaired the effect (Supplemental Fig. 6F; Fig. 6**A–D**). To obtain insights into how ALKBH5 stimulated the fibroblast-to-myofibroblast transformation, the effects of ALKBH5 overexpression and knockdown were examined on the myofibroblast phenotype. RT-qPCR showed that ALKBH5 overexpression increased the mRNA expression levels of fibroblast-to-myofibroblast transformation markers, *Col1α1*, *α-SMA*, *Fn*, and *Ctgf*, whereas ALKBH5 knockdown reduced these levels (Supplemental Fig. 6G). Of note, we found that ALKBH5 overexpression resulted in significant traces of α-SMA in fibroblasts, indicating that the cells had differentiated into myofibroblasts (Fig. 6**E**). In contrast, fibroblasts transduced with Ad-sh-ALKBH5 exhibited little α-SMA expression compared with those transduced with Ad-sh-Control (Fig. 6**E**). Western blot analysis confirmed that ALKBH5 overexpression upregulated Col1α1 and α-SMA protein levels in fibroblasts under both normoxia and hypoxia, whereas ALKBH5 knockdown reduced the expression of these proteins (Fig. 6**F**).

Altogether, these results indicated that ALKBH5 enhanced the proliferative and migratory capacities of fibroblasts and accelerated their transformation into myofibroblasts, thus clarifying the novel molecular mechanism of hypoxia-induced fibroblast-to-myofibroblast transformation.

ALKBH5 regulated transcripts associated with repair after acute MI via m6A demethylation

To explore the m6A demethylated targets of ALKBH5 in response to acute MI, MeRIP-seq and RNA-seq were performed using RNA isolated from the infarct areas of ALKBH5-KO and WT mice 5 days after MI surgery (WT, n = 3 vs. KO, n = 3). Analysis of representative motifs (5′-RRACW-3′; R = A or G, W = A or U) from

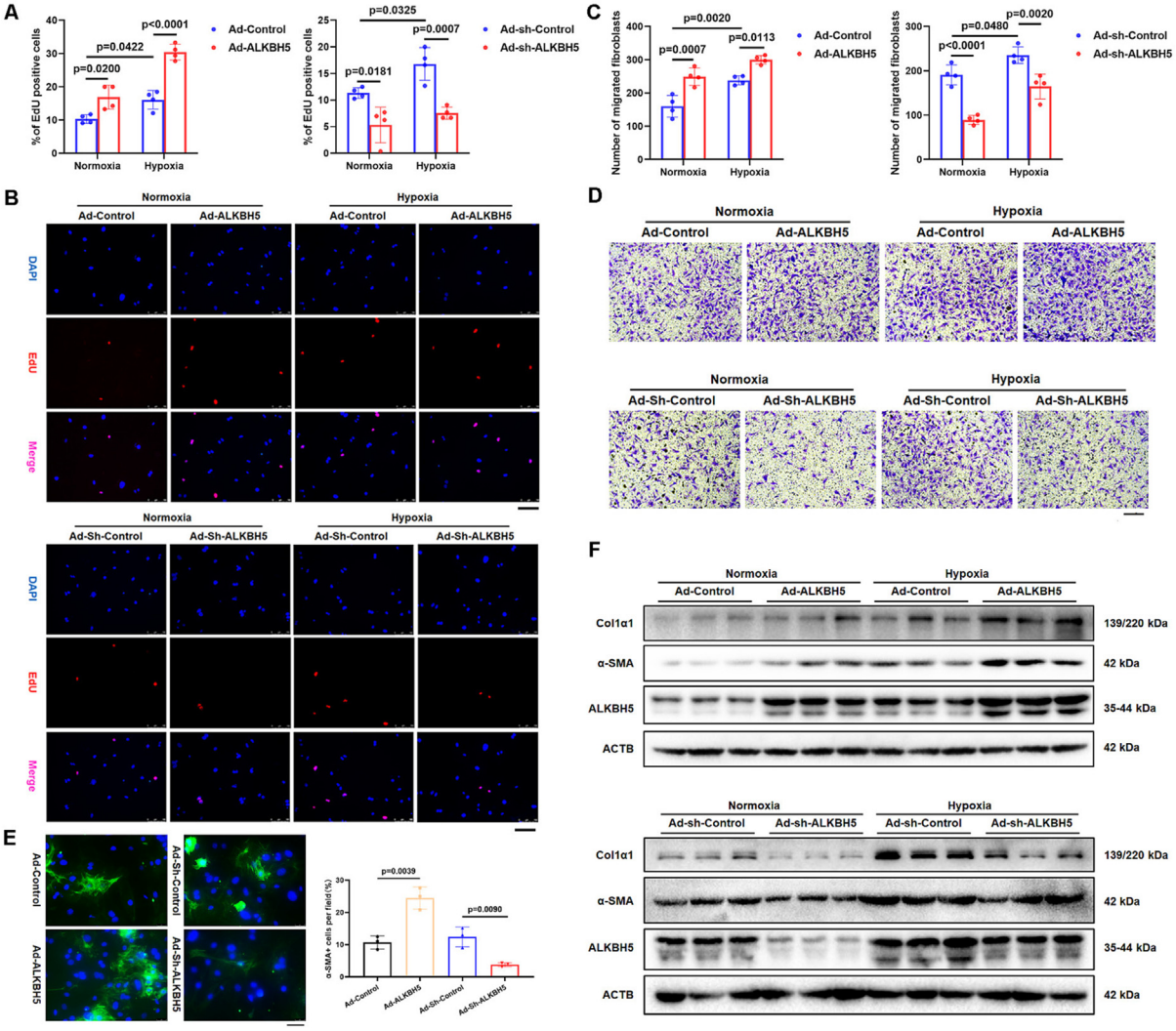

Fig. 6. The role of ALKBH5 in fibroblast proliferation, migration and induction of FMT Fibroblasts were treated by Ad-Control, Ad-ALKBH5, Ad-Sh-Control, or Ad-Sh-ALKBH5 for 24 h. Then fibroblasts were cultured in normoxia or hypoxia for 48 h. **(A)**EdU analysis of the proportion of EdU (green) and DAPI (blue) double-positive cell in DAPI positive cell (n = 4 per group, Two-Way ANOVA using Tukey's multiple comparisons test). **(B)** EdU assay. Fibroblasts in the S-phase were stained with EdU in green while the nuclei were stained with DAPI in blue. Scale bars, 25 μm. **(C)** The number of migrated fibroblasts (n = 4 per group, Two-Way ANOVA using Tukey's multiple comparisons test). **(D)** Representative images and quantification of migrated fibroblasts. Scale bar, 200 μm. **(E)** Representative images of immunofluorescence staining with α-SMA in green and DAPI in blue (n = 3 per group, Unpaired two-tailed Student's *t*-test). Scale bars, 25 μm. **(F)** The protein levels of α-SMA, Col1α1, ALKBH5 and ACTB were measured by Western blot. (For interpretation of the references to colour in this figure legend, the reader is referred to the web version of this article.)

the WT and KO groups was performed, which was consistent with the previously identified m6A recognition sequences (Fig. 7**A**). Differential transcriptome-wide methylation was mainly observed within the terminator region and the 3′-UTR binding sites of *Alkbh5* (Fig. 7**B and 7C**). RNA-seq revealed that 439 genes were upregulated and 1,032 genes were downregulated in the ALKBH5-KO mice compared with the WT mice, whereas MeRIP-seq analysis identified 954 hypomethylated and 414 hypermethylated peaks (Fig. 7**D**). KEGG enrichment analysis using RNA-seq (Fig. 7**E**) and MeRIP-seq (Fig. 7**F**) data suggested major signaling pathways related to the EGFR pathway, including the tyrosine kinase, calcium, PI3K/AKT, and ErbB signaling pathways. Furthermore, GO enrichment analysis using RNA-seq (Fig. 7**E**) and MeRIP-seq (Fig. 7**F**) data revealed a common subset of transcripts that were largely associated with scar repair, the extracellular matrix, cell differentiation, cell proliferation, and receptor tyrosine kinase signaling. Further evaluation of the mRNA and m6A modification levels of the corresponding genes indicated that ALKBH5 affected the expression of many genes via m6A demethylation during the early stage of MI**,** including the extracellular matrix-related genes, *Col4a4, Col6a6,* and *St14* (Fig. 7**G).** A four-quadrant scatter plot was used for a more in-depth data analysis, and the function of each of the four distinct subgroups has been shown in Supplemental Fig. 7. Considering ALKBH5 as a demethylase, we screened for genes with hypermethylation and differential alteration in the ALKBH5-KO and WT groups (Fig. 7**H**). Further analysis revealed genes with differential m6A modification between the ALKBH5-KO and WT groups. Consistent with the significant enrichment of the EGFR signaling pathway identified by the KEGG and GO enrichment analyses, erb-b2 receptor tyrosine kinase 4 (*ErbB4*), a member of the receptor tyrosine protein kinase family and epidermal growth factor receptor sub-family, was also identified as a potential target of ALKBH5 in this analysis (Fig. 7**I**). In contrast to the downregulation of *ErbB4* expression in the ALKBH5-KO group, tumorigenicity 14 (*St14*), a gene encoding an extracellular matrix enzyme, was upregulated. It was also identified as a possible downstream target of ALKBH5 (Fig. 7**H**). These data were further supported using MeRIP-seq, which showed significant enrichment of ALKBH5-induced m6A demethylation in the terminal fragments of *ErbB4* and *St14*. In contrast, ALKBH5 knockdown resulted in the upregu-

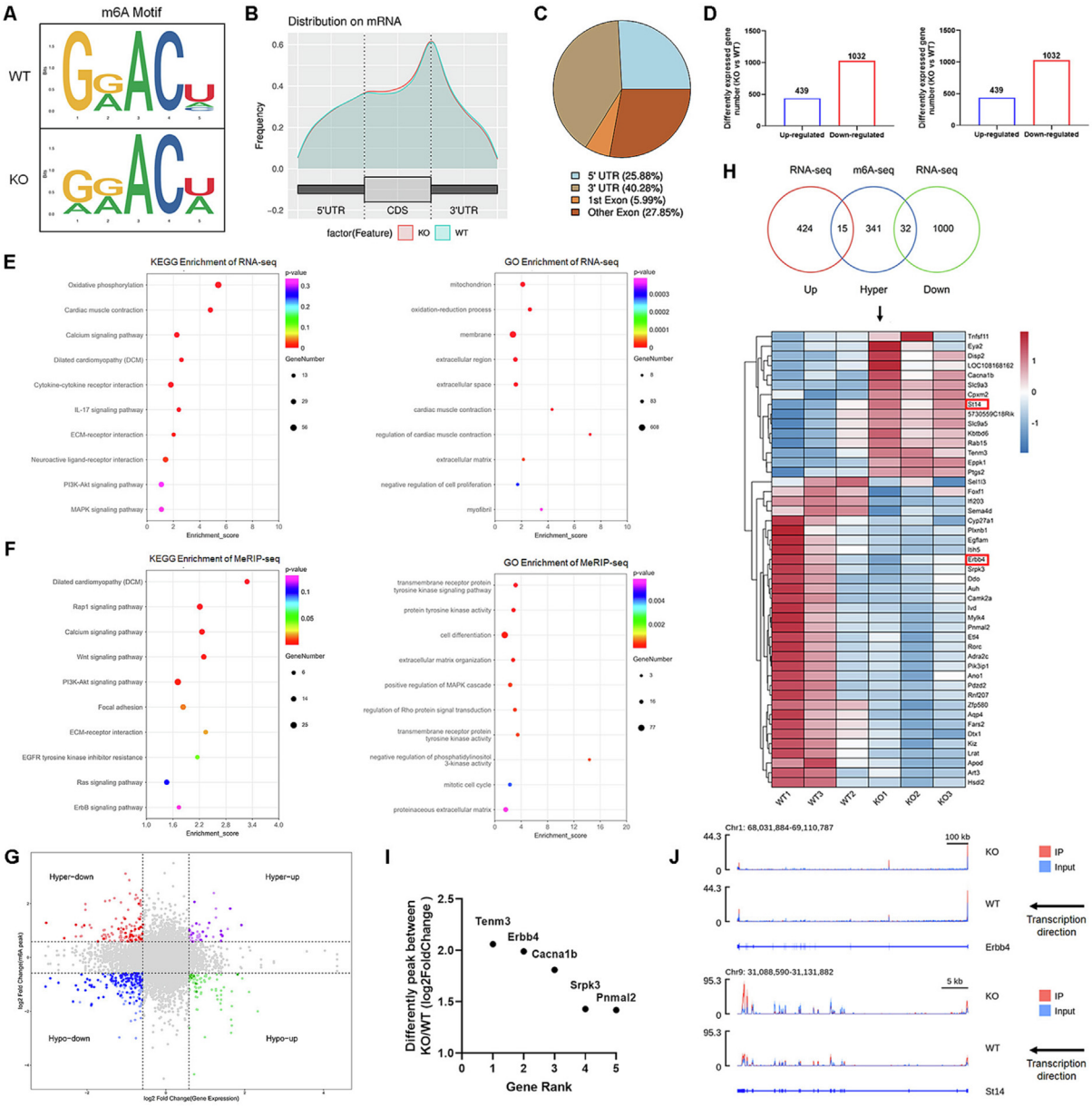

Fig. 7. Transcripts in AMI are regulated by ALKBH5 mediated m6A modification (A) Analysis of representative motifs from the WT and KO. **(B)** Guitar plot showing the distribution of m6A peaks on mRNA transcripts. **(C)** Pie chart showing the differential distribution of m6A peaks on mRNA transcripts. **(D)** Bar chart showing the numbers of differentially gene expression and m6A peaks between the WT and KO groups. KEGG enrichment analysis and Go enrichment analysis by **(E)** RNA-seq and **(F)** MeRIP-seq. **(G)** The four-quadrant scatter plot showed the distribution of mRNA expression and m6A methylation levels of the gene. **(H)** Screening strategy of differential transcripts (P > 0.05, Fold Change > 1.5 or < 0.67). **(I)** The index of the different peak of log2FoldChange between KO and WT groups represented the different enrichment level of the top five genes. **(J)** Integrated genome browser views of the m6A peaks on ErbB4 and ST14.

lation of m6A-modified fragments, indicating that the downregulation of *ErbB4* mRNA levels and upregulation of *St14* mRNA levels were mediated via m6A modification in an ALKBH5-dependent manner (Fig. 7**J**).

ALKBH5 regulated ErbB4 and St14 expression via m6A demethylation

Adenoviral modification of ALKBH5 expression in fibroblasts was used to confirm *ErbB4* and *St14* as downstream targets of ALKBH5. ALKBH5 overexpression led to increased *Alkbh5, ErbB4, Col4a4*, and *Col6a6* mRNA levels and decreased *St14* mRNA levels, whereas ALKBH5 knockdown resulted in the opposite effect on these mRNA levels (Fig. 8**A and 8B**). Similar changes were observed in the hypoxic cell model. Hypoxia upregulated *Alkbh5, ErbB4, St14, Col4a4*, and *Col6a6* mRNA levels, and ALKBH5 overexpression further upregulated *Alkbh5, ErbB4, Col4a4*, and *Col6a6* mRNA levels. However, ALKBH5 knockdown inhibited the hypoxia-induced upregulation of *Alkbh5, ErbB4*, and *Col6a6* mRNA levels (Fig. 8**A and 8B**). ALKBH5 overexpression inhibited the hypoxia-induced upregulation of *St14* mRNA levels, whereas ALKBH5 knockdown further upregulated its mRNA levels (Fig. 8**A and 8B**). Our data demonstrated that ALKBH5 regulated *ErbB4* and *St14* expression at the transcriptional level.

Next, we screened for m6A sites in *ErbB4* and *St14* mRNA using MeRIP-seq and the RMBase database. The potential m6A-modified sites in *ErbB4* and *St14* mRNA were enriched near the terminator region, which was located in the CDS region of *ErbB4* and the 3′-UTR of *St14* (Supplemental Fig. 8A). This was consistent with our

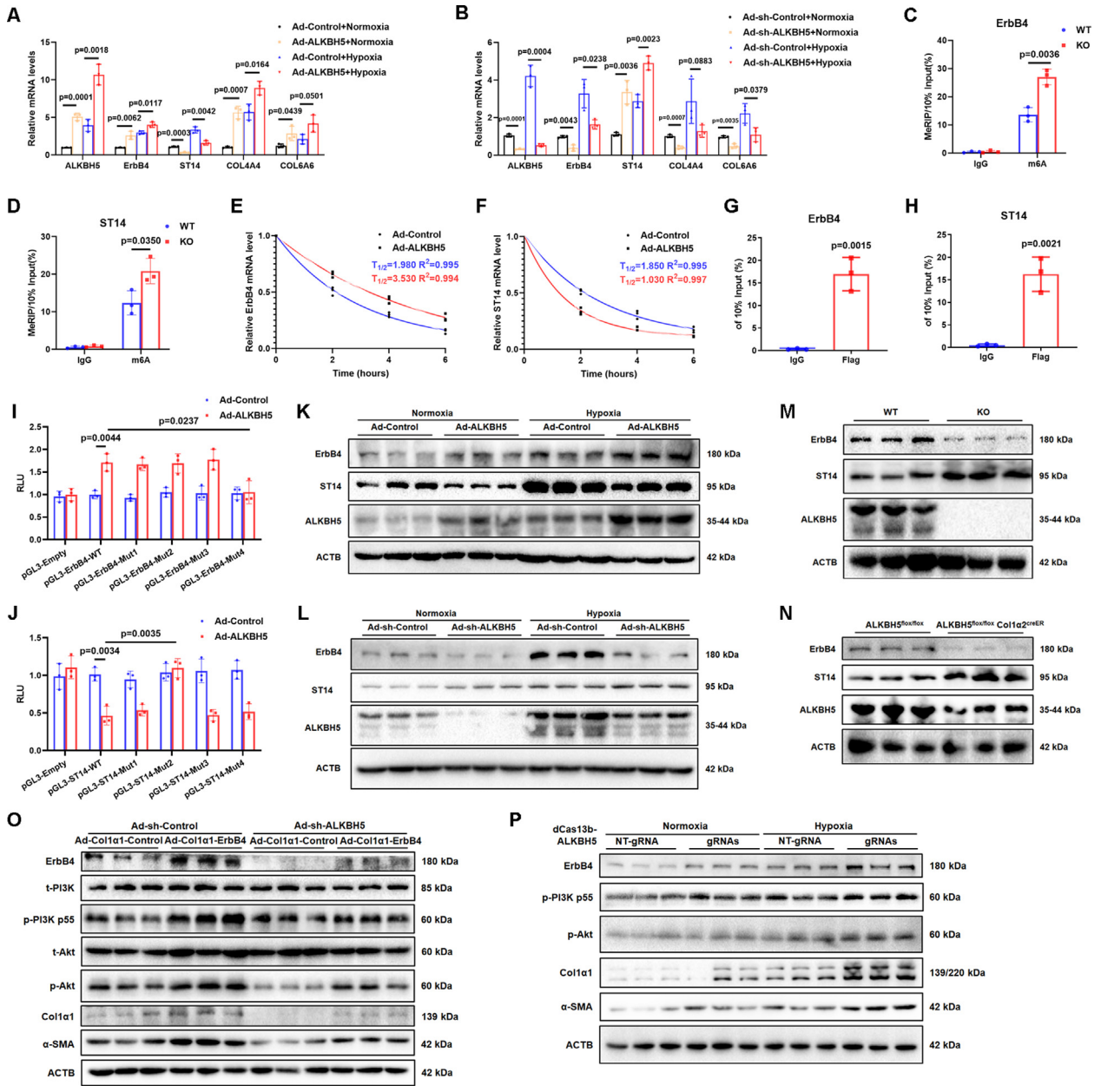

Fig. 8. ALKBH5 accelerated fibroblast activation via m6A demethylation of ErbB4 mRNA Fibroblasts were treated by Ad-Sh-Control + Normoxia, Ad-Sh-ALKBH5 + Normixia and Ad-Sh-Control + Hypoxia, Ad-Sh-ALKBH5 + Hypoxia. **(A and B)** RT-qPCR analysis of ALKBH5, ErbB4, ST14, Col4a4 and Col6a6 mRNA levels (n = 3 per group, Unpaired two-tailed Student's *t*-test). MeRIP-qPCR quantitative analysis of the fold enrichment of **(C)** ErbB4 (ErbB4-CDS) and **(D)** ST14 (ST14-3′UTR) m6A level by immunoprecipitation with specific m6A antibody in fibroblasts isolated from WT mice and KO mice (n = 3 per group, Unpaired two-tailed Student's *t*-test). Fibroblasts were treated by Ad-Control + Actinomycin D or Ad-ALKBH5 + Actinomycin D. RT-qPCR analysis of **(E)** ErbB4 and **(F)** ST14 levels at 0,2,4,6 h and the mRNA level of ErbB4 and ST14 at 0 h as control (n = 3 per group, non-linear regression curve fitting [one phase decay]). **(G and H)** RIP products were measured by RT-qPCR (n = 3 per group, Unpaired two-tailed Student's *t*-test). **(I and J)** Dual-luciferase reporter assay after cotransfection with the reporter vector and Ad-ALKBH5 or Ad-Control in NIH/3T3 cells for 48 h (n = 3 per group, Unpaired two-tailed Student's *t*-test). **(K and L)** Western blot analysis of ALKBH5, ErbB4, ST14 and ACTB protein levels in fibroblasts. Representative Western blot image of ALKBH5, ErbB4, ErbB4 and ACTB protein level from **(M)** KO group and **(N)** cKO group at day 5 post-MI compared with respective control. **(O)** Representative Western blot showing ErB4, ACTB, α-SMA, t-Akt, t-PI3K, p-Akt, p-PI3K p55 and Col1α1 protein levels. **(P)** Representative Western blot showing ErB4, ACTB, α-SMA, p-Akt, p-PI3K p55 and Col1α1 protein levels.

MeRIP-seq data and previous findings [17,18]. The m6A-modified sites enriched in the CDS and 3′-UTR, especially near the terminator, were closely related to mRNA stability [19].

MeRIP was performed in cardiac fibroblasts isolated from WT and ALKBH5-KO mice using IgG control antibody or anti-m6A antibody. Immunoprecipitation with the anti-m6A antibody resulted in highly enriched mRNA levels of *ErbB4* (*ErbB4*-CDS) and *St14* (*St14*-3′-UTR) compared with those obtained with the IgG control antibody. However, the mRNA levels of *ErbB4*-5′-UTR, *ErbB4*-3′-UTR, *St14*-5′-UTR, and *St14*-CDS were not affected. Additionally, the m6A levels were more significantly enriched in *ErbB4* (*ErbB4*-CDS) and *St14* (*St14*-3′-UTR) in the ALKBH5-KO group than the WT group (Fig. 8**C and 8D;** Supplemental Fig. 8B). This was consistent with our MeRIP-seq data (Fig. 7**J**). Our results collectively suggested that m6A modification was involved in the regulation of *ErbB4* and *St14* expression via ALKBH5.

ALKBH5 m6A demethylation has been shown to affect mRNA stability [20], indicating that ALKBH5 may possibly affect the sta-

bility of *ErbB4* and *St14* mRNA. Therefore, after ALKBH5 overexpression, we examined the *ErbB4* and *St14* mRNA levels at 0, 2, 4, and 6 h after inhibiting RNA polymerase via actinomycin D treatment. RT-qPCR assay demonstrated that overexpressed ALKBH5 elevated the half-life of *ErbB4* mRNA in contrast to the control group, whereas it reduced the half-life of *St14* mRNA, indicating that ALKBH5 stabilized *ErbB4* mRNA and destabilized *St14* mRNA **(**Fig. 8**E and 8F)**. Interestingly, because ALKBH5 exhibited opposite effects on the stabilization of *ErbB4* and *St14* mRNA, the m6A-modified sites of *ErbB4* and *St14* may be recognized by different m6A readers. To determine any direct interaction between ALKBH5 and *ErbB4* or *St14* mRNA, RNA-IP assay was performed using an anti-FLAG or IgG control antibody in cardiac fibroblasts transduced with an adenoviral FLAG-tagged ALKBH5 vector (Ad-ALKBH5). Immunoprecipitation with the anti-FLAG antibody resulted in enriched levels of *ErbB4* and *St14* mRNA compared with those obtained with the IgG control antibody **(**Supplemental Fig. 9A**;** Fig. 8**G and 8H)**. To verify the specific m6A sites targeted by ALKBH5 in *ErbB4* and *St14* mRNA, we constructed luciferase reporter vectors containing the wild-type (pGL3-*ErbB4*-WT) or mutated (pGL3-*ErbB4*-Mut1,2,3,4) coding sequence of *ErbB4* mRNA or containing the wild-type (pGL3-*St14*-WT) or mutated (pGL3-*St14*-Mut1,2,3,4) 3′-UTR sequence of *St14* mRNA **(**Supplemental Fig. 8C**)**. Dual-luciferase reporter assays showed that ALKBH5 overexpression enhanced the luciferase activity of pGL3-ErbB4-WT and pGL3-ErbB4-Mut1,2,3 **(**Fig. 8**I)**. In contrast, ALKBH5 overexpression decreased the luciferase activity of pGL3-ST14-WT and pGL3-ST14-Mut1,3,4 and had no effect on pGL3-ST14-Mut2 **(**Fig. 8**J)**. Furthermore, it was demonstrated that the fourth potential m6A site (Mut4) in *ErbB4* mRNA and the second potential m6A site (Mut2) in *St14* mRNA were ALKBH5-mediated demethylation sites. Next, we preliminarily explored which m6A readers may or may not affect the stability of *ErbB4* and *St14* mRNA. Currently, YTHDF2/3 and IGF2BP1/2/3 are the main m6A readers that can effectively regulate RNA degradation and stabilization, respectively [21,22]. Therefore, we constructed small interfering RNAs to target YTHDF2/3 and IGF2BP1/2/3. RT-qPCR showed that IGF2BP2 regulated the stabilization of *ErbB4* mRNA via m6A demethylation, whereas YTHDF2 was involved in the degradation of *St14* mRNA **(**Supplemental Fig. 9B and 9C**)**. Altogether, we found that ALKBH5 increased the stabilization of *ErbB4* mRNA and degradation of *St14* mRNA via m6A demethylation.

The regulation of *ErbB4* and *St14* expression via ALKBH5 at the protein level was assessed *in vivo and in vitro*. We transduced cardiac fibroblasts with modified adenoviruses under normoxic or hypoxic conditions. ALKBH5 overexpression upregulated ErbB4 protein levels, which were further upregulated under hypoxic conditions. In contrast, ALKBH5 knockdown downregulated ErbB4 protein levels under normoxic conditions and also inhibited the hypoxia-mediated upregulation of ErbB4 **(**Fig. 8**K and 8L)**. ALKBH5 overexpression downregulated ST14 protein levels and also inhibited the hypoxia-mediated upregulation of ST14. Conversely, ALKBH5 knockdown upregulated ST14 protein levels and reinforced the hypoxia-mediated upregulation of ST14 **(**Fig. 8**K and 8L)**. Additionally, reduced ALKBH5 and ErbB4 protein levels and elevated ST14 protein levels were detected in the infarct areas of the ALKBH5-KO and fibroblast-specific ALKBH5-KO mice 5 days after MI surgery in contrast to those of the control mice **(**Fig. 8**M and 8N)**.

ALKBH5 accelerated fibroblast-to-myofibroblast transformation via m6A demethylation of ErbB4 mRNA

Here, we explored whether or not ALKBH5 knockdown inhibited fibroblast-to-myofibroblast transformation as a result of decreased ErbB4 expression. We generated an ErbB4-overexpression adenoviral vector containing the fibroblast-specific *Col1α1* promoter (Ad-Col1α1-ErbB4) to specifically upregulate ErbB4 in cardiac fibroblasts. The overexpression efficiency of Ad-Col1α1-ErbB4 was confirmed by RT-qPCR **(**Supplemental Fig. 9D**).** ALKBH5 knockdown markedly decreased the levels of α-SMA and Col1α1; however, this effect was inhibited after transduction with Ad-Col1α1-ErbB4 **(**Fig. 8**O)**. Similar downstream changes were observed in PI3K/AKT signaling **(**Fig. 8**O)**. To confirm whether ALKBH5 promotes the phenotypic transformation of fibroblasts via m6A demethylation of *ErbB4* mRNA, NIH/3T3 cells were transfected with dCas13b-ALKBH5 and gRNAs (gRNA 1–3) targeting *ErbB4* mRNA. The construction strategy and working diagram of dCas13b-ALKBH5 have been provided as Supplemental Fig. 9E**.** RT-qPCR showed that transfection with dCas13b-ALKBH5 and the gRNAs significantly upregulated *ErbB4* mRNA levels compared with the control (NT-gRNA) (Supplemental Fig. 9E). The protein levels of ErbB4, p-PI3K, p-AKT, α-SMA, and Col1α1 were also significantly upregulated after transfection with dCas13b-ALKBH5 and the gRNAs. Hypoxia stimulation further upregulated the expression of these proteins (Fig. 8**P**). These data suggested that ALKBH5 promoted the fibroblast-to-myofibroblast transformation via upregulated ErbB4 expression. Next, we estimated the protective role of ALKBH5/ErbB4 axis on cardiomyocytes against hypoxic injury. Western blot results showed ALKBH5 deletion inhibited ErbB4 expression in cardiomyocytes, but not in ECs **(**Supplemental Fig. 9H**)**. Tunel staining showed ALKBH5 deficiency aggravated cardiomyocyte apoptosis induced by hypoxia which could be partly reversed by ErbB4 overexpression (Ad-ErbB4) **(**Supplemental Fig. 9I**)**.

Fibroblast-specific ErbB4 overexpression by in situ adenoviral injection prevented cardiac rupture and improved post-MI repair and cardiac function in mice

We next investigated the therapeutic potential of fibroblast ErbB4 on post-MI repair and cardiac function via myocardial injection of Ad-Col1α1-ErbB4 or Ad-Col1α1-Control in ALKBH5$^{flox/flox}$-Col1α2^{creER} mice 30 min after MI surgery **(**Fig. 9**A)**. The fibroblast-specific ErbB4 overexpression improved the overall survival rate (59.3%, n = 27 vs. 85.7%, n = 28) and cardiac rupture ratio (9/27 vs. 3/28) of the ALKBH5$^{flox/flox}$Col1α2^{creER} mice after MI surgery **(**Fig. 9**B and 9C)**. Western blot confirmed that Ad-Col1α1-ErbB4 injection increased ErbB4 expression, peaked on day 7 post-MI and returned to baseline levels on day 21 post-MI (Fig. 9**D**). To assess infarct repair, Col1α1 and α-SMA protein levels were examined by Western blot **(**Fig. 9**E and 9F)** and Collagen I, Collagen III levels were examined by immunofluorescence (Fig. 9**G**) on day 5 post-MI. The mice injected with Ad-Col1α1-ErbB4 demonstrated improved post-MI repair compared with the mice injected with Ad-Col1α1-Control. Specifically, these mice exhibited significantly more collagen deposition and a higher overall minimum wall thickness than the control mice **(**Fig. 9**H and 9I)**. Echocardiography further indicated that Ad-Col1α1-ErbB4 injection ameliorated left ventricular dilation and cardiac function post-MI **(**Fig. 9**J)**. Altogether, the transient overexpression of ErbB4 in fibroblasts significantly prevented cardiac rupture and improved infarct repair and cardiac function after MI.

Discussion

MI occurs as a result of coronary artery occlusion, which may subsequently lead to a series of serious complications, including fatal arrhythmia and cardiac rupture [1,23]. Here, we have elucidated the effect of ALKBH5-mediated m6A demethylation in cardiac remodeling following MI. Our research has demonstrated

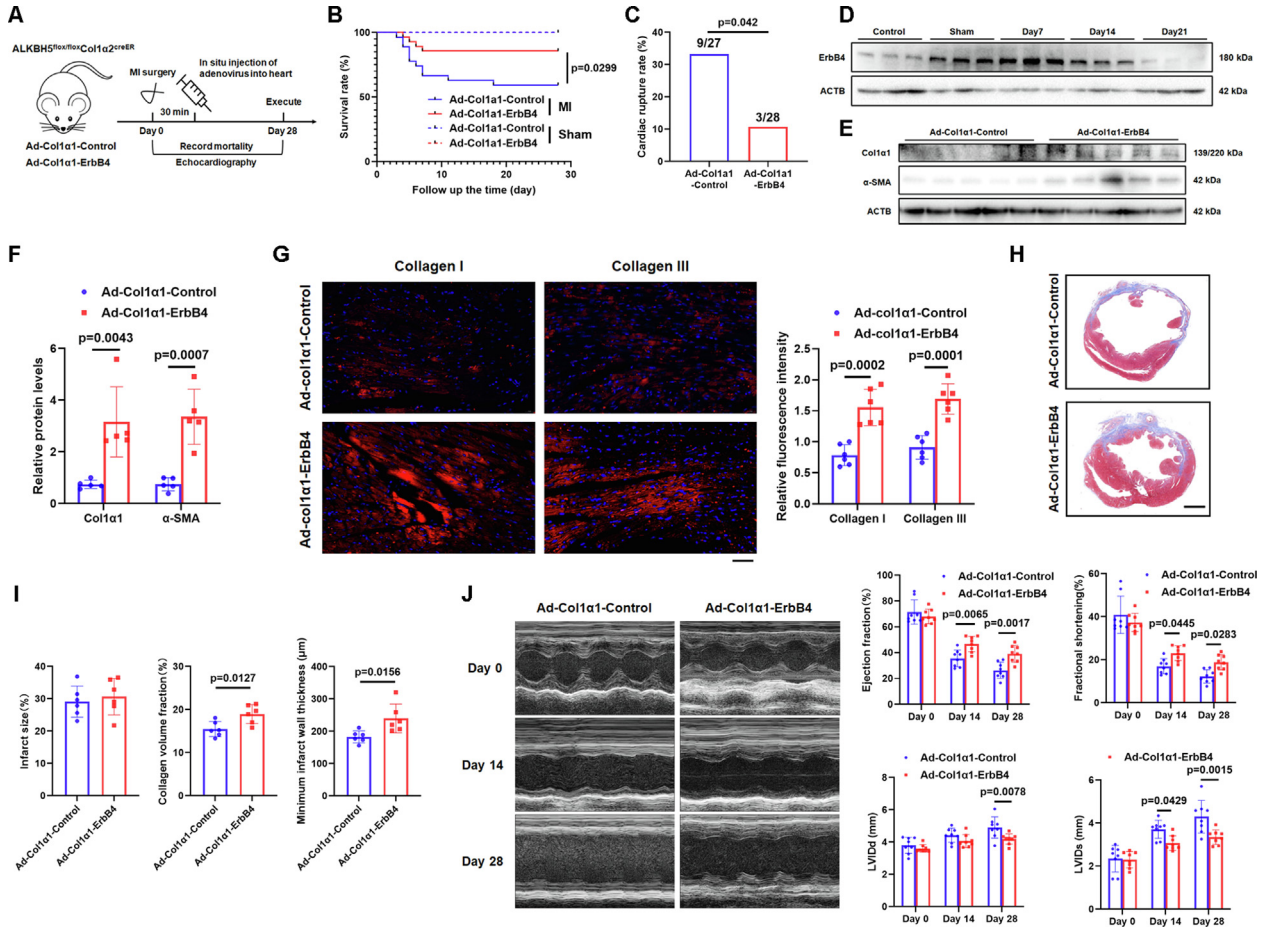

Fig. 9. ErbB4 overexpression in fibroblasts by adenovirus in situ injection prevents cardiac rupture, improves infarct repair and cardiac function in mice After MI Left coronary artery ligation surgery was performed in ALKBH5$^{flox/flox}$Col1α2^{creER} mice, then cardiac in situ virus injection 30 min after operation. (n = 27 in Ad-Col1α1-Control group and n = 28 in Ad-Col1α1-ErbB4 group). **(A)** Experimental strategy of myocardial infarction model in Ad-Col1α1-Control group and Ad-Col1α1-ErbB4 group. (**B**) The survival curve (Ad-Col1α1-Control group n = 27 vs Ad-Col1α1-ErbB4 group n = 28, Log-rank test) and of and **(C)** the occurrence of cardiac rupture-induced death in Ad-Col1α1-Control group and Ad-Col1α1-ErbB4 group from the day of left coronary artery ligation until postoperative 28 days (chi-square test). **(D)** The Western blot analysis of adenovirus delivery efficiency. **(E and F)** The protein levels of Col1α1 and α-SMA were measured in the infarct area of hearts of Ad-Col1α1-Control group and Ad-Col1α1-ErbB4 group 5 days after MI by Western blot analysis (n = 5 per group, Unpaired two-tailed Student's *t*-test). **(G)** Representative diagram and quantification of fluorescence intensity of collagen I and collagen III (n = 6 per group, Unpaired two-tailed Student's *t*-test). Scale bars, 50 μm. **(H)** Representative images of Masson's trichrome staining of ventricular sections of ALKBH5$^{flox/flox}$ group and ALKBH5$^{flox/flox}$Col1α2^{creER} group 28 days after myocardial infarction and **(I)** the analysis of infarct size, collagen volume fraction and minimum wall thickness (n = 6 per group, Unpaired two-tailed Student's *t*-test).Scale bars, 1 mm. **(J)** Echocardiography was performed to assess EF, FS, LVIDd and LVIDs of the left ventricle in Ad-Col1α1-Control group and Ad-Col1α1-ErbB4 group at days sham 14 and 28 post-MI (n = 8 per group, Two-Way ANOVA using Šídák's multiple comparisons test).

fibroblast ALKBH5 not only as a key regulator of cardiac remodeling but also as a protective factor from cardiac rupture post-MI. This novel discovery involving the HIF-1α/ALKBH5/ErbB4 axis might provide novel treatment targets for the prevention of post-MI cardiac rupture (Fig. 10).

The m6A methylation is the most abundant and essential RNA modification, and it has become a popular area of research in cardiovascular science [24]. We found that the m6A levels decreased in the border and infarct areas and then began to rise, which was consistent with the findings by Mathiyalagan [8]. Similarly, the m6A methylation in cardiac fibroblasts increased significantly in response to hypoxia. Furthermore, we analyzed the *in vivo and in vitro* expression of various m6A methyltransferase and demethylases, and the most significant changes were observed in m6A demethylase ALKBH5 expression.

Ventricular wall rupture represents one of the most fatal complications of MI in the clinic [25,26]. Although it is believed that the incidence of post-MI cardiac rupture is relatively low, autopsies have confirmed that cardiac rupture causes 24% of deaths after MI [25,26]. It is urgent to illuminate the molecular mechanisms of post-MI cardiac rupture to making prevention policy. In our study, ALKBH5 deficiency led to a higher overall mortality rate and incidence of cardiac rupture compared with WT mice. Furthermore, ALKBH5 deficiency resulted in worse scar repair after MI, despite a similar infarct size, as well as exacerbated ventricular wall thinning and cardiac dysfunction. These *in vivo* results suggest that ALKBH5 is indispensable during post-MI cardiac remodeling and that its deficiency results in an increased occurrence of cardiac rupture during the early stage of MI and exacerbated damage to cardiac structure and function during the later stage of MI. Furthermore, the global ALKBH5-KI mice exhibited reduced infarct size and improved cardiac function without exacerbated cardiac fibrosis after MI. However, the occurrence of cardiac rupture and death was not reduced. Han et al. [12] have recently reported the ALKBH5/m6A/YTHDF1/YAP axis in the mediation of cardiomyocyte proliferation and heart regeneration and that ALKBH5 overexpression improves cardiac function post-MI. Therefore, we speculate that the cardioprotective role of ALKBH5 after MI may be through the improvement of cardiomyocyte function and survival and thus may not be limited to only fibroblasts. Here, our promising *in vivo*

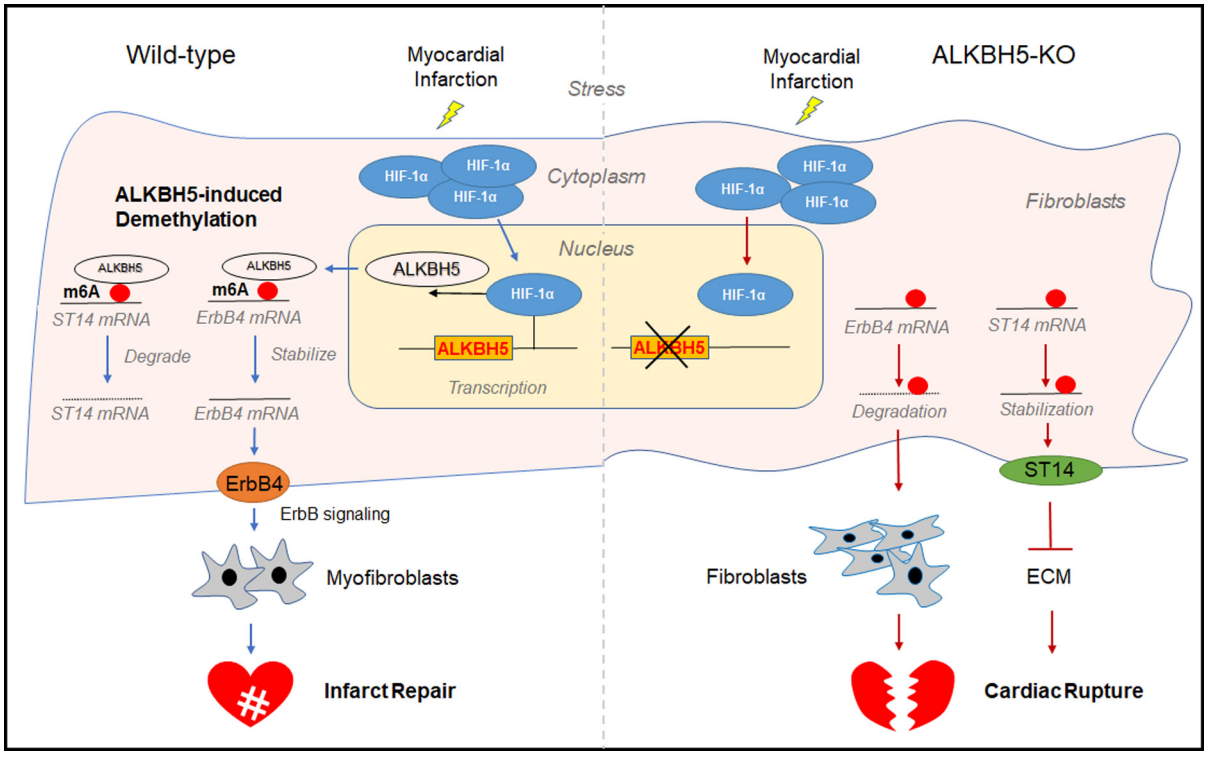

Fig. 10. The HIF-1α/ALKBH5/ErbB4 and ST14 pathway regulates cardiac rupture post-MI. Our study reinforces ALKBH5 as a potential therapeutic target for ischemic heart diseases by the mechanisms that the HIF-1α/ALKBH5/ErbB4 and ST14 pathway regulates post-MI cardiac rupture and hypoxia-induced cardiac fibroblast-to-myofibroblast transformation.

results suggest that interventions targeting ALKBH5 may be an effective and safe treatment to prevent cardiac rupture and improve cardiac remodeling post-MI.

It is unknown exactly which factors are responsible for the increased occurrence of cardiac rupture in the ALKBH5-KO mice in contrast to the WT mice. Inflammation-mediated phagocytosis of necrotic myocardial cells and fibroblast-mediated scar formation is essential to the repair phase after MI [23,27,28]. The proliferative fibroblasts directly promote scar maturation, thus playing an important effect in post-MI cardiac repair [29]. In this study, significantly less collagen and fewer proliferating myofibroblasts were observed in the infarct border and infarct areas of the ALKBH5-KO mice after MI surgery in contrast to those of the WT mice. This explained the poor post-MI scar formation observed in the ALKBH5-KO mice. We further demonstrated that ALKBH5 deficiency promoted cardiac rupture by inhibiting fibroblast activation in the early stage of MI using our fibroblast-specific ALKBH5-KO mice. Consistent with our previous results, fibroblast-specific ALKBH5 knockout resulted in an increased overall cardiac rupture rate, worse adverse cardiac remodeling, and deteriorated cardiac function. The novelty of the current research is the identification of the effect of ALKBH5 in cardiac fibroblasts during early scar repair after MI. An excessive and prolonged inflammatory response in the infarct area may impair scar formation and cause cardiac rupture [30]. Indeed, we observed that post-MI inflammation was somehow affected by ALKBH5 knockout because a reduced number of $CD68^+$ macrophages was observed in the infarct areas of mice 3 days post-MI, whereas a reduced number of $Ly6G^+$ neutrophils was observed in the infarct border areas. Nonetheless, the effect of ALKBH5 in the inflammation after MI was not the main focus of this study. However, this is something that we will pursue in our future research on ALKBH5. ALKBH5 knockout mice showed improved angiogenesis than WT mice post MI, which was consistent with the results of our published article [12], in that loss of ALKBH5 promoted post-ischemic angiogenesis, however, improved angiogenesis did not prevent cardiac rupture post MI. Thus, angiogenesis might only play a minor role in cardiac rupture in our study setting. It is important to note that several different cardiac cell populations are likely to contribute to the post-MI processes, and the contribution of ALKBH5 during cardiac adaptation and in the regulation of fibroblast function, as described here, may only be part of these processes.

Our data demonstrated hypoxia, but not other critical stimuli, as a driver of fibroblast differentiation. Furthermore, hypoxia resulted in a significant upregulation of ALKBH5 in fibroblasts at the transcriptional level via HIF-1α. Consistent with our findings, previous researchers have reported that hypoxia upregulates ALKBH5 expression in breast cancer cells and Escherichia coli via HIF-1α-induced transcriptional regulation [14,15]. Zhang *et al.* have determined that transcription factor EB binds to the *ALKBH5* promoter to activate its transcription during autophagy [11]. Currently, there is more focus on m6A demethylase FTO than ALKBH5 in many research fields [8,31,32]. The identification of these different crucial transcription factors modulating ALKBH5 expression indicates that ALKBH5 is involved in various pathological events, which greatly warrants further in-depth study. Our *in vitro* results also demonstrated that ALKBH5 expression improved the proliferative and migratory capacities of fibroblasts and promoted the fibroblast-to-myofibroblast transformation in response to hypoxia, whereas the opposite effects were observed with ALKBH5 knockdown. Altogether, our study has identified that ALKBH5 is hypoxia-mediated activator of cardiac fibroblasts. METTL3 has also been reported to regulate TGF-β induced cardiac fibrosis and the fibroblast-to-myofibroblast transition [33]. It seems to contradict our results that both an m6A writer and eraser can promote the activation of fibroblasts. However, we speculate that these contradictory results may be due to the different timepoints after MI, in which these factors play their respective roles. In support of this

speculation, we have shown that ALKBH5 responds to hypoxia and promotes scar repair during the early stage of MI, whereas TGF-β-induced METTL3 exacerbates fibrosis in the late stage of MI.

ALKBH5 has been identified in fibroblast-induced cardiac repair after MI; however, it is still unclear how ALKBH5 functions via an m6A modification-dependent manner. Transcriptome differential expression analysis and m6A profiling of the infarct area tissues from WT and ALKBH5-KO mice 5 days after MI surgery were used to uncover the various transcripts involved in the post-MI repair processes, including extracellular matrix deposition, cell differentiation, and proliferation. These results explain why we observed an increased frequency of cardiac rupture as well as poor scar formation in the ALKBH5-KO mice after MI surgery. Furthermore, we screened out the transcription factors ErbB4 and ST14 as potential targets from RNA-seq and MeRIP-seq. Our data suggested that ALKBH5 showed the opposite effects in affecting the stability of *ErbB4* and *St14* mRNA via m6A demethylation. For instance, ALKBH5 is shown to improve the mRNA stability of *YTHDF1* and increase its expression by m6A demethylation [12], whereas ALKBH5 inhibits angiogenesis by destabilization of *WNT5A* mRNA [13]. The mechanisms in which different m6A readers are involved, including that of ALKBH5-m6A mediated *ErbB4* and *St14* mRNA stabilization/destabilization, will continue to be studied in the future.

ST14/matriptase is an epithelium-derived membrane serine protease and induces extracellular matrix degradation [34,35]. Our *in vivo and in vitro* data revealed elevated ST14 expression in response to ALKBH5 deficiency in the myocardial tissues of mice and cardiac fibroblasts, which may explain the increased MMP levels in the ALKBH5-KO mice post-MI. The function of ErbBs in the heart is puzzling because both positive and negative effects have been reported in different studies [36,37]. Manabu et al. [38] have reported that ErbB2 and ErbB4 are expressed in fibroblasts after MI and that blocking ErbB function significantly accelerates cardiac fibroblast senescence and apoptosis. ErbB2, ErbB3, and ErbB4 are expressed in human cardiac ventricular fibroblasts, and NRG-1β could enhance the proliferation and viability of fibroblasts via ErbBs/PI3K/AKT signaling [39]. Whereas, Galindo et al. [40] have shown that NRG-1β attenuates cardiac fibrosis and inhibits myofibroblasts and extracellular matrix formation in a swine MI model. In our study, fibroblast-specific overexpression of ErbB4 ameliorated the ALKBH5 knockout-mediated inhibition of cardiac fibroblast activation via PI3K/AKT signaling, poor collagen repair, the increased occurrence of cardiac rupture, and cardiac dysfunction post-MI. Altogether, these findings support that elevated ErbB4 expression via ALKBH5-induced m6A demethylation is essential for the activation of fibroblasts in the early stage of MI. Fibroblast-specific overexpression of ErbB4 is a potential post-MI therapy to promote infarct healing and prevent cardiac rupture.

Study limitations

In this study, our findings revealed the protective effects of ALKBH5/ErbB4 overexpression against post-MI cardiac rupture and dysfunction. However, these findings were only demonstrated in animal models. Therefore, additional studies using clinical patient data are needed to validate our findings and achieve early clinical translation.

Conclusions

In summary, this study has uncovered a novel link between cardiac rupture and m6A demethylase ALKBH5. By elucidating the mechanisms by which the HIF-1α/ALKBH5/ErbB4 pathway regulates post-MI cardiac rupture and hypoxia-induced cardiac fibroblast-to-myofibroblast transformation, our study has reinforced ALKBH5/ErbB4 as potential therapeutic targets for treating MI.

CRediT authorship contribution statement

Kun Yang: Conceptualization, Data curation, Investigation, Methodology, Formal analysis, Writing – original draft. **Yongchao Zhao:** Investigation, Validation, Funding acquisition, Writing – review & editing. **Jingjing Hu:** Investigation, Validation, Funding acquisition, Writing – review & editing. **Rifeng Gao:** Investigation, Validation, Writing – review & editing, Formal analysis, Formal analysis. **Jiaran Shi:** Investigation, Writing – review & editing, Formal analysis. **Xiang Wei:** Investigation, Writing – review & editing. **Juntao Chen:** Investigation, Writing – review & editing. **Kai Hu:** Methodology, Writing – review & editing. **Aijun Sun:** Conceptualization, Methodology, Resources, Writing – original draft, Project administration, Funding acquisition. **Junbo Ge:** Conceptualization, Methodology, Resources, Writing – original draft, Project administration.

Declaration of Competing Interest

The authors declare that they have no known competing financial interests or personal relationships that could have appeared to influence the work reported in this paper.

Acknowledgements

The authors appreciate all the individuals and clinicians for their participation in this study. The authors all thank for the important support from Professor Shaorong Gao from Tongji University and Professor Hongsheng Wang from Sun Yat-sen University.

This study was supported by a grant to Aijun Sun from key project of the National Natural Science Foundation of China (82130010), the National Science Fund for Distinguished Young Scholars (81725002), the fellowship of China National Postdoctoral Program for Innovative Talents (BX20220094), the China Postdoctoral Science Foundation (2022M710776), the Shanghai Municipal Science and Technology Major Project (2017SHZDZX01), the Innovation Program of Shanghai Municipal Education Commission (2021 Science and Technology Creation-03-1); a grant to Yongchao Zhao from the Basic Research Program of the Department of Science and Technology of Guizhou Province (Qiankehe Foundation-ZK [2022] General 671); and a grant to Jingjing Hu from Medical and Health Science and Technology Plan Project of Zhejiang Province (2023RC160).

Appendix A. Supplementary material

Supplementary data to this article can be found online at https://doi.org/10.1016/j.jare.2023.09.004.

References

[1] Pouleur A-C, Barkoudah E, Uno H, Skali H, Finn PV, Zelenkofske SL, et al. Pathogenesis of sudden unexpected death in a clinical trial of patients with myocardial infarction and left ventricular dysfunction, heart failure, or both. Circulation 2010;122(6):597–602.

[2] Omiya S, Omori Y, Taneike M, Protti A, Yamaguchi O, Akira S, et al. Toll-like receptor 9 prevents cardiac rupture after myocardial infarction in mice independently of inflammation. Am J Phys Heart Circ Phys 2016;311(6):H1485–97.

[3] Jia D, Jiang H, Weng X, Wu J, Bai P, Yang W, et al. Interleukin-35 promotes macrophage survival and improves wound healing after myocardial infarction in mice. Circ Res 2019;124(9):1323–36.

[4] Heck AM, Wilusz CJ. Small changes, big implications: the impact of m(6)A RNA methylation on gene expression in pluripotency and development. BBA 2019;1862(9):194402.
[5] Li J, Yang X, Qi Z, Sang Y, Liu Y, Xu B, et al. The role of mRNA m(6)A methylation in the nervous system. Cell Biosci 2019;9(1).
[6] Longenecker JZ, Gilbert CJ, Golubeva VA, Martens CR, Accornero F. Epitranscriptomics in the heart: a focus on m(6)A. Curr Heart Fail Rep 2020;17(5):205–12.
[7] Tong J, Flavell RA, Li HB. RNA m(6)A modification and its function in diseases. Front Med 2018;12(4):481–9.
[8] Mathiyalagan P, Adamiak M, Mayourian J, Sassi Y, Liang Y, Agarwal N, et al. FTO-dependent N(6)-methyladenosine regulates cardiac function during remodeling and repair. Circulation 2019;139(4):518–32.
[9] Berulava T, Buchholz E, Elerdashvili V, Pena T, Islam MR, Lbik D, et al. Changes in m6A RNA methylation contribute to heart failure progression by modulating translation. Eur J Heart Fail 2020;22(1):54–66.
[10] Dorn LE, Lasman L, Chen J, Xu X, Hund TJ, Medvedovic M, et al. The N(6)-methyladenosine mRNA methylase METTL3 controls cardiac homeostasis and hypertrophy. Circulation 2019;139(4):533–45.
[11] Song H, Feng X, Zhang H, Luo Y, Huang J, Lin M, et al. METTL3 and ALKBH5 oppositely regulate m(6)A modification of TFEB mRNA, which dictates the fate of hypoxia/reoxygenation-treated cardiomyocytes. Autophagy 2019;15(8):1419–37.
[12] Han Z, Wang X, Xu Z, Cao Y, Gong R, Yu Y, et al. ALKBH5 regulates cardiomyocyte proliferation and heart regeneration by demethylating the mRNA of YTHDF1. Theranostics 2021;11(6):3000–16.
[13] Zhao Y, Hu J, Sun X, Yang K, Yang L, Kong L, et al. Loss of m6A demethylase ALKBH5 promotes post-ischemic angiogenesis via post-transcriptional stabilization of WNT5A. Clin Transl Med 2021;11(5):e402.
[14] Zhang C, Samanta D, Lu H, Bullen JW, Zhang H, Chen I, et al. Hypoxia induces the breast cancer stem cell phenotype by HIF-dependent and ALKBH5-mediated m(6)A-demethylation of NANOG mRNA. PNAS 2016;113(14).
[15] Thalhammer A, Bencokova Z, Poole R, Loenarz C, Adam J, O'Flaherty L, et al. Human AlkB homologue 5 is a nuclear 2-oxoglutarate dependent oxygenase and a direct target of hypoxia-inducible factor 1alpha (HIF-1alpha). PLoS One 2011;6(1):e16210.
[16] Guimaraes-Camboa N, Stowe J, Aneas I, Sakabe N, Cattaneo P, Henderson L, et al. HIF1alpha represses cell stress pathways to allow proliferation of hypoxic fetal cardiomyocytes. Dev Cell 2015;33(5):507–21.
[17] Dominissini D, Moshitch-Moshkovitz S, Schwartz S, Salmon-Divon M, Ungar L, Osenberg S, et al. Topology of the human and mouse m6A RNA methylomes revealed by m6A-seq. Nature 2012;485(7397):201–6.
[18] Zhang H, Shi X, Huang T, Zhao X, Chen W, Gu N, et al. Dynamic landscape and evolution of m6A methylation in human. *Nucleic Acids Res* 2020; 48(11): 6251-64.
[19] Huang H, Weng H, Chen J. m(6)A modification in coding and non-coding RNAs: roles and therapeutic implications in cancer. Cancer Cell 2020;37(3):270–88.
[20] Tang C, Klukovich R, Peng H, Wang Z, Yu T, Zhang Y, et al. ALKBH5-dependent m6A demethylation controls splicing and stability of long 3'-UTR mRNAs in male germ cells. PNAS 2018;115(2).
[21] Shi H, Wei J, He C. Where, when, and how: context-dependent functions of RNA methylation writers, readers, and erasers. Mol Cell 2019;74(4):640–50.
[22] Jiang X, Liu B, Nie Z, Duan L, Xiong Q, Jin Z, et al. The role of m6A modification in the biological functions and diseases. Signal Transduct Target Ther 2021;6(1).
[23] Thackeray JT, Hupe HC, Wang Y, Bankstahl JP, Berding G, Ross TL, et al. Myocardial inflammation predicts remodeling and neuroinflammation after myocardial infarction. J Am Coll Cardiol 2018;71(3):263–75.
[24] Hinger SA, Wei J, Dorn LE, Whitson BA, Janssen PML, He C, et al. Remodeling of the m(6)A landscape in the heart reveals few conserved post-transcriptional events underlying cardiomyocyte hypertrophy. J Mol Cell Cardiol 2021;151:46–55.
[25] Matteucci M, Fina D, Jiritano F, Meani P, Blankesteijn WM, Raffa GM, et al. Treatment strategies for post-infarction left ventricular free-wall rupture. Eur Heart J Acute Cardiovasc Care 2019;8(4):379–87.
[26] Gao XM, White DA, Dart AM, Du XJ. Post-infarct cardiac rupture: recent insights on pathogenesis and therapeutic interventions. Pharmacol Ther 2012;134(2):156–79.
[27] Shinde AV, Frangogiannis NG. Fibroblasts in myocardial infarction: a role in inflammation and repair. J Mol Cell Cardiol 2014;70:74–82.
[28] Wang X, Guo Z, Ding Z, Inflammation MJL. Autophagy, and apoptosis after myocardial infarction. J Am Heart Assoc 2018;7(9).
[29] van den Borne SW, Diez J, Blankesteijn WM, Verjans J, Hofstra L, Narula J. Myocardial remodeling after infarction: the role of myofibroblasts. Nat Rev Cardiol 2010;7(1):30–7.
[30] Frangogiannis NG, Rosenzweig A. Regulation of the inflammatory response in cardiac repair. Circ Res 2012;110(1):159–73.
[31] Yang S, Wei J, Cui Y-H, Park G, Shah P, Deng Yu, et al. m(6)A mRNA demethylase FTO regulates melanoma tumorigenicity and response to anti-PD-1 blockade. Nat Commun 2019;10(1).
[32] Deng X, Su R, Weng H, Huang H, Li Z, Chen J. RNA N(6)-methyladenosine modification in cancers: current status and perspectives. Cell Res 2018;28(5):507–17.
[33] Li T, Zhuang Y, Yang W, Xie Y, Shang W, Su S, et al. Silencing of METTL3 attenuates cardiac fibrosis induced by myocardial infarction via inhibiting the activation of cardiac fibroblasts. FASEB J 2021;35(2):e21162.
[34] Wang Y, Rathinam R, Walch A, Alahari SK. ST14 (suppression of tumorigenicity 14) gene is a target for miR-27b, and the inhibitory effect of ST14 on cell growth is independent of miR-27b regulation. J Biol Chem 2009;284(34):23094–106.
[35] Tsui KH, Chang PL, Feng TH, Chung LC, Sung HC, Juang HH. Evaluating the function of matriptase and N-acetylglucosaminyltransferase V in prostate cancer metastasis. Anticancer Res 2008;28(4A):1993–9.
[36] Falls DL. Neuregulins: functions, forms, and signaling strategies. Exp Cell Res 2003;284(1):14–30.
[37] Yarden Y, Sliwkowski MX. Untangling the ErbB signalling network. Nat Rev Mol Cell Biol 2001;2(2):127–37.
[38] Shiraishi M, Yamaguchi A, Suzuki K. Nrg1/ErbB signaling-mediated regulation of fibrosis after myocardial infarction. FASEB J 2022;36(2):e22150.
[39] Kirabo A, Ryzhov S, Gupte M, Sengsayadeth S, Gumina RJ, Sawyer DB, et al. Neuregulin-1beta induces proliferation, survival and paracrine signaling in normal human cardiac ventricular fibroblasts. J Mol Cell Cardiol 2017;105:59–69.
[40] Galindo CL, Kasasbeh E, Murphy A, Ryzhov S, Lenihan S, Ahmad FA, et al. Anti-remodeling and anti-fibrotic effects of the neuregulin-1beta glial growth factor 2 in a large animal model of heart failure. J Am Heart Assoc 2014;3(5):e000773.